CHALMERS
UNIVERSITY OF TECHNOLOGY

Aerodynamic optimization of pylons to improve rear wing performance using passive and active systems

Master's thesis in Automotive engineering

Avaneesh Upadhyaya
Kaushik Nagaraja Rao

DEPARTMENT OF MECHANICS AND
MARITIME SCIENCES

CHALMERS UNIVERSITY OF TECHNOLOGY
Gothenburg, Sweden 2021
www.chalmers.se

MASTER'S THESIS IN AUTOMOTIVE ENGINEERING

Aerodynamic optimization of pylons to improve rear wing performance using passive and active systems

AVANEESH UPADHYAYA
KAUSHIK NAGARAJA RAO

Department of Mechanics and Maritime Sciences
Division of Vehicle Engineering and Autonomous Systems (VEAS)
CHALMERS UNIVERSITY OF TECHNOLOGY

Göteborg, Sweden 2021

Aerodynamic optimization of pylons to improve rear wing performance using passive and active systems
AVANEESH UPADHYAYA
KAUSHIK NAGARAJA RAO

Master's thesis 2021:15
Department of Mechanics and Maritime Sciences
Division of Vehicle Engineering and Autonomous Systems (VEAS)
Chalmers University of Technology
SE-412 96 Göteborg
Sweden
Telephone: +46 (0)31-772 1000

Supervisor: Magnus Urquhart, Department of Mechanics and Maritime Sciences
Supervisor: Ugo Riccio, Automobili Lamborghini S.p.A
Supervisor: Vincenzo Sepe, Automobili Lamborghini S.p.A
Examiner: Simone Sebben, Department of Mechanics and Maritime Sciences

Cover:
Aventador Superveloce[1]

Chalmers Reproservice
Göteborg, Sweden 2021

Aerodynamic optimization of pylons to improve rear wing performance using passive and active systems
Master's thesis in Automotive Engineering
AVANEESH UPADHYAYA
KAUSHIK NAGARAJA RAO
Department of Mechanics and Maritime Sciences
Division of Vehicle Engineering and Autonomous Systems (VEAS)
Chalmers University of Technology

Abstract

In collaboration with Automobili Lamborghini S.p.A, an aerodynamic investigation was carried out on a dual pylon rear wing assembly to improve cornering stability of a car at high speeds. The pylon's primary purpose is to provide structural support to the wing. However, this project aimed at improving the performance of Aventador SV's rear wing using aerodynamically optimized pylons that not only boosted its downforce generating capabilities, but also generated large side forces at higher yaw angles.

The project goals were fulfilled in two phases. The first phase involved development of pylon airfoils that would keep the flow attached within a range of ± 15 yaw angles, without augmenting the drag when compared to NACA0010. A surrogate based model was used to generate these airfoils. 2D simulations were performed on the airfoils along with passive and active systems to achieve attached flow around the pylons, thus, generating more downforce by improving suction under the wing. Single slot approach was used to create passive slots that improved flow on one side of the design at the expense of the other. The active flow control was implemented in two ways, blowing and suction. Throughout this study, active blowing has held precedence due to energy constraints. Three airfoils with better performance than NACA0010 at higher yaw angles were selected for next phase.

In the second phase, airfoils from 2D study were used to carry out 3D simulations using RANS solver on several wing and pylon combinations, without a car body, in a quest to find the optimum performing pylon. A study was conducted to analyse the effect of different pylon positions, sizes, and profiles along with passive and active systems on the air flow around the wing. With the profiles generated in 2D study, an improvement in the performance of the wing was achieved at higher yaw angles. Wherever the flow detached over the pylon, passive and active systems showed signs of improvement.

Keywords: Pylons, Rear Wing, Aerodynamics, Asymmetric Airfoil, Low Reynolds, Lift, Drag, CFD, Passive, Active, STAR-CCM+

Acknowledgements

We would like to express our utmost gratitude to our supervisor Magnus Urquhart at Chalmers for their patient guidance and supervision throughout the thesis. The thesis would not have progressed as far as it did without his useful and constructive recommendations. Thank you Magnus for generously devoting your time to our questions. We would like to extend our gratitude towards our industry supervisors Ugo Riccio and Vincenzo Sepe at Automobili Lamborghini S.p.A for their valuable critiques and insights to guide us in the right direction. We appreciate the time and effort you invested in us and we thoroughly enjoyed working alongside you. Completing this project would not have been possible without the kind support and encouragement provided by our examiner Simone Sebben. Thank you for ensuring that this project proceeded without any hurdles.

Contents

List of Figures

List of Tables

1 Introduction

The margin between the lap timings of performance cars is getting narrower by the day. To battle these narrow margins, care must be given to the smallest of the parts which may be overlooked at times. One such area can be the pylon section of a rear wing that connects to the car. A thorough study on the implementation of active flow controls and passive slotted designs to the pylons could bring out potential performance improvements, in this case, cornering performance.

Automobili Lamborghini S.p.A is one of the foremost super sports cars manufacturers in the world, and since their innovative system of active aerodynamics, Aerodinamica Lamborghini Attiva (ALA)[2] took hold, the concept of super sports cars performance has been taken to levels not seen before. The rear wings of the cars with ALA system equipped, work on the principal of active flow control to improve performance of the vehicle[3][4]. The rear wing on the cars is used to generate large amounts of downforce, helping the vehicle to stay on track at higher speeds. The downforce generation is exceptionally important while executing turns. Improving the downforce can enhance the car's cornering speeds and therefore the lap timings. Although this effect is beneficial for achieving faster lap times, it comes with a penalty of higher drag force. Designing the car's rear wing for a better cornering performance and downforce improvement with very little drag penalty can be a bit challenging. In this thesis, pylons would be redesigned to compensate for changes in the yaw angles, making the rear wing more robust against the higher yaw angles. A detached flow under the wing hampers the performance significantly. This upgrade is expected to improve the performance in two ways. First, improve flow around the suction side of the wing, creating more downforce. Second, generate forces in the lateral direction to improve cornering stability. The scope for air yaw angle in this study ranges from $-15°$ to $+15°$ based on an investigation performed by Oskar Hellsten & Oskar Pettersson[5] for high performance car.

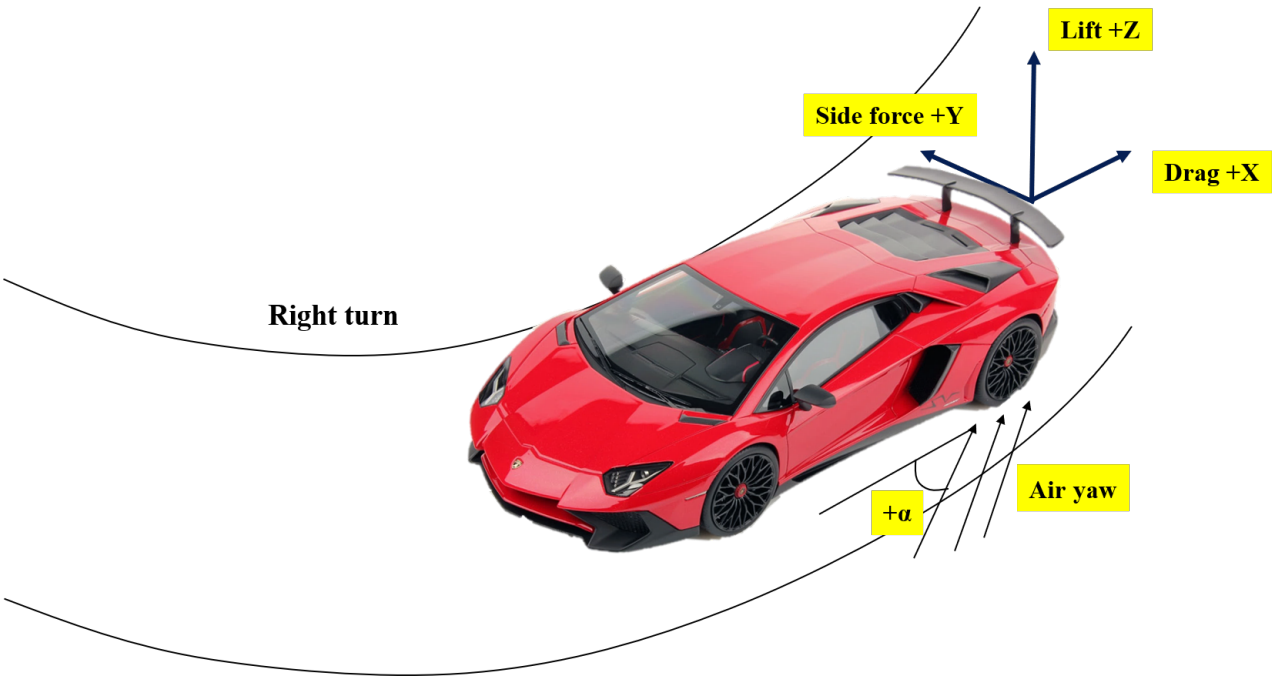

Figure 1.1: *Schematic showing relative air yaw while cornering*

Figure 1.1 is annotated to explain how the study was carried out on the rear wing of Lamborghini Aventador SV. When a car is cornering, in this case taking a right turn, the yaw moment about car center would pull the front of the car into the corner but push the rear outwards. Due to this, the relative motion between the wing and air is rotated that generated forces in +X and +Y directions. The coordinate system used throughout this thesis was a local coordinate system that moves with the car. For this thesis, the convention maintained was that the car taking a right turn resulted in a positive yaw angle flow, and the right pylon would be the one downstream and placed over the inner wheels. Ensuring high downforce over the inner wheels is of utmost importance during cornering. Figure 1.2 provides a greater insight into the area of focus. It has a representative

cross-section of the pylon and not the actual cross-section of the pylons. Lamborghini Aventador SV has a dual pylon wing assembly, making it symmetric. Thus, an asymmetric airfoil which required a study performed in positive and negative yaw angles, when converted to a 3D pylon along with the wing was simulated for only positive yaw angles. Cross-section of the pylon was optimized during the 2D study to ensure attached flow around the pylons. While, only the wing and pylon assemblies were considered in 3D study.

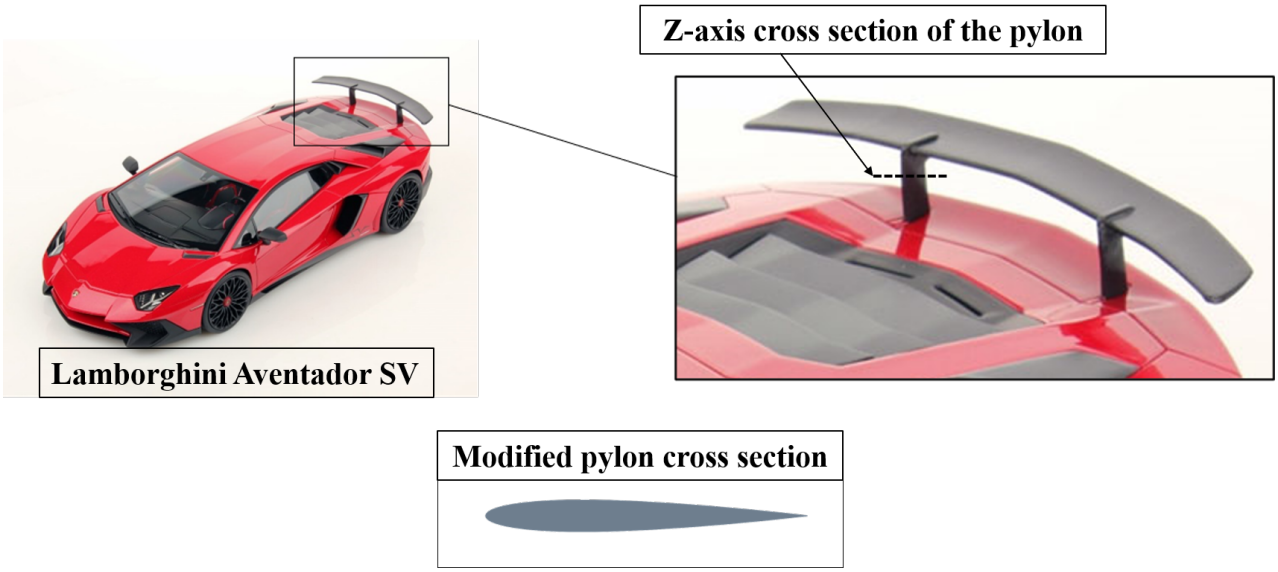

Figure 1.2: *Focus areas for 3D and 2D studies*

1.1 Purpose

The objective of this master thesis was to propose new pylon designs for the wing and to perform aerodynamic studies introducing passive and active flow control measures for performance optimization. As no optimization work was carried out on the wing in this thesis, the goal of the proposed pylon designs was to match or improve the downforce generated by the wing without pylons, while mitigating drag penalties at lower yaw angles. The scope for the pylon studies ranges from yaw angles between +15° to -15°. This thesis also addressed the following questions;

- Can asymmetric airfoils produce better averaged lift forces than symmetric airfoils in the local coordinate system?
- How does the geometry and positioning of the passive or active system affect performance of the airfoil?
- What are the pros and cons of passive and active systems?
- Why was a single slot passive system implemented over dual slot?
- Can a single slot passive system perform well in positive as well as negative yaw conditions?
- How does the size, placement and the geometry of the pylon affect the performance of the rear wing?
- Do the results from the 2D airfoil study correlate to the results obtained from 3D wing and pylon study?
- Is it necessary to use active and passive systems to maintain attached flow within the yaw angle scope?

1.2 Literature Study

This thesis is a successor to another master thesis performed in 2020 by Oskar Hellsten & Oskar Pettersson, titled 'A novel approach to the design of rear airfoil pylons on high performance car'[5]. The focus of the previous thesis was on symmetric airfoils and the implementation of passive systems for flow improvement,

which provided a good foundation to build upon. Based on their work, NACA0010 was chosen as the reference airfoil for this thesis. Even after optimising symmetric airfoils for low drag performance, NACA0010 was undefeated at lower yaw angles. However, the trade-off for this airfoil was the stalling at high yaw angles. For the airfoil study in this thesis, a low Reynolds number (≈ 695000) was chosen. A study performed on NACA0009 and NACA0012 to understand the airfoil characteristics at low Reynolds number[6] provided deeper insights into the performance expectations of NACA0010. The simulations backed by experimental correlation helped shape the approach for designing optimum airfoils for this thesis.

Theory of Wing Sections[7] provided the initial overview of this topic. The plethora of airfoil data documented in this book along with the literature on passive systems were crucial for our airfoil designs. Another interesting concept for improving flow using a passive system was achieved by introducing a small notch over NACA4412[8]. However, this concept reduced the separations but unable to maintain attached flow at higher angles of attack. The book Competition Car Aerodynamics[9] was extremely helpful and gave a general idea about wing designs and parameters. It also helped to define the range of airfoil design parameters for optimizing asymmetric airfoils. Most of the asymmetric airfoils researched online produced good lift in one direction, but stalled early in the other direction. As our use case was dependant on maximum average lift, most of the research on asymmetric airfoils did not meet our criterion. Some of the common airfoils like NACA0012, NACA2412, NACA4415 and NACA63-215 performed similar to NACA0010 at lower yaw angles when the values were averaged for positive and negative angles of attack. This comparison was made possible through the vast data available on Airfoil Tools[10]. In this thesis, we used the two coordinate systems to our advantage by allowing the asymmetric airfoils to have global rotation as well. Thus, the airfoil chords need not align with the X direction.

The airfoil studies are generally performed using a global coordinate system, where the airfoil is rotated by said angle of attack and the flow direction is kept constant along with the coordinate system. Thus, the airfoil would not lie along the coordinate system at an angle greater than 0°. However, in this thesis, a local coordinate system was implemented by keeping the airfoil fixed, while the air flow was rotated to simulate the yaw angle. The Figure 1.3 shows the differences between the two systems when an angle of attack exists. The +X and +Y axes are fixed and denote drag and lift forces respectively. When the first approach is used, both the drag and lift forces increase when the angle of attack is increased, until the airfoil stalls. This was noticed through the airfoil data presented in the book Theory of Wing Sections mentioned above and also through Airfoil Tools[10]. However, when the local coordinate system was used, the drag forces started to decrease as the yaw angle increased. While, the lift continued to increase. Again, this held true until the wing stalled. After stalling, the lift forces reduced while the drag force increased.

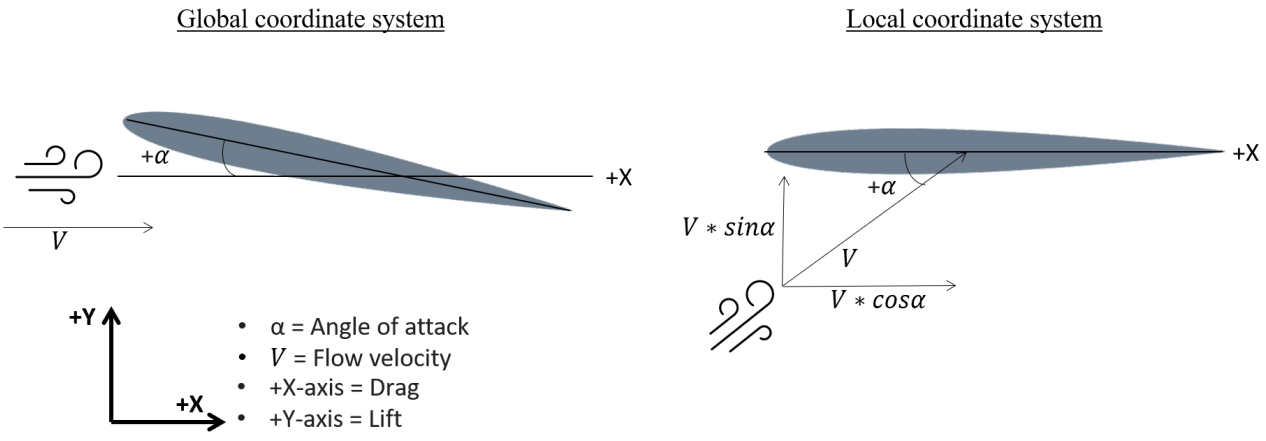

Figure 1.3: *Global and local coordinate systems annotated on NACA0010*

The geometry and simulation pictures presented in this report were taken from STAR-CCM+[11], while all the plots reported were generated using MATLAB[12].

1.3 Limitations

As the thesis is spanned for 20 weeks, the duration of the project is a major limitation. The quest to find an optimum pylon design is a long process and is time bounded. The following points may be considered as limitations for this thesis;

- 3D simulations on the wing and pylon combinations were carried out without a car body, and were suspended mid air.
- By using Reynolds Averaged Navier Stokes solver, we were unable to see the effect of active and passive systems in real time. On a race track, the yaw angles vary rapidly, and it is important that the passive and active systems can operate efficiently to meet such demands.
- Active flow control implemented had a fixed flow rate, and could not be increased to significantly improve the robustness against high angle of attack.
- Manufacturing capabilities were considered while designing the airfoil, especially for fillets. This proved to hinder the performance when compared to a completely conceptual airfoil design.
- The pylons were optimized aerodynamically and did not undergo any structural tests. However, the designs are not impractical as they have been discussed and agreed upon by experienced supervisors.

2 Airfoil Study

This chapter explains the pylon airfoil geometry considerations, computational domain size, boundary conditions and other details related to the CFD pre-processes for a two-dimensional study of airfoils. Furthermore, details regarding the passive and active flow controls will be described. This section focuses on the study related to the pylon's airfoil geometry in 2D. This 2D study stands as a base for the 3D pylons used in Section 4.

2.1 Simulation Overview

To carry out any CFD simulations it is essential to define a flow region or the domain size. The size of the domain must be chosen in such a way that it captures all the necessary flow interaction without being very large. A larger domain size comes with a consequence of longer simulation run times and higher computational costs. After careful considerations, a computational domain of 8m width ($\approx$ 30 times the chord length) and 14m length ($\approx$ 50 times the chord length) was implemented as seen in Figure 2.1. The model was placed at a distance of $4m$ along the X-axis from the flow inlet boundary, and midway of the $8m$ width (Y-axis).

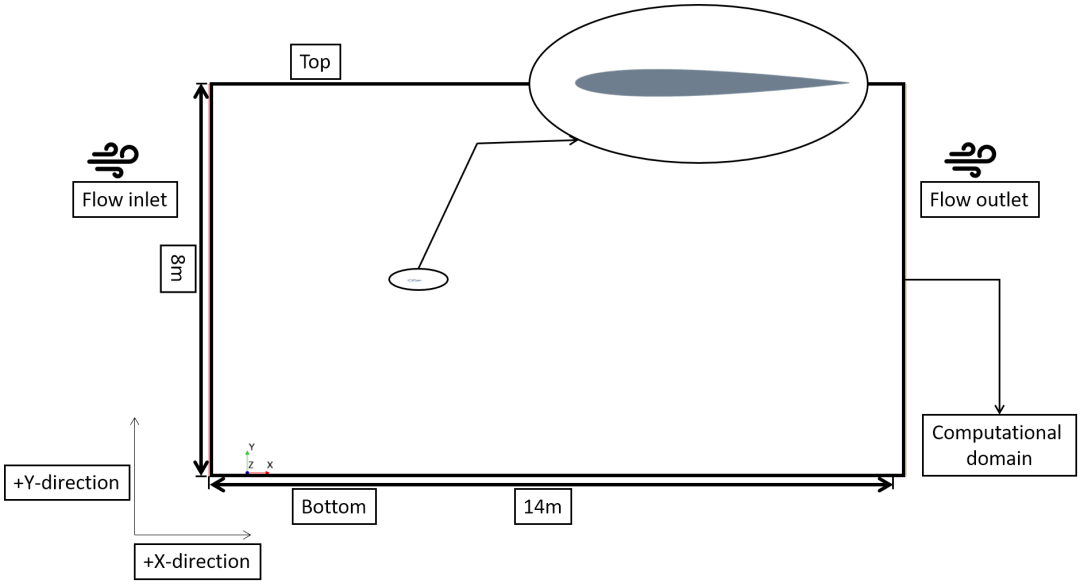

Figure 2.1: *Domain size*

2.1.1 Coordinate System & Force Coefficients

The coordinate system used for the 2D studies is shown in Figure 2.2. Positive X-direction is towards the outlet of the domain and positive Y-direction is towards the top of the domain. The drag of the airfoil is considered to be in the positive X-direction and the lift is measured in the Y-direction. The positive and negative lift follows the same sign convention as the Y-axis (positive Y-axis has a positive lift and vice-versa). Lift of the airfoil becomes the side force of the car and the drag remains the same. The equations for the non-dimensional force coefficients are mentioned below.

$$C_D = \frac{2 * F_x}{\rho * v^2 * A} \qquad (2.1) \qquad\qquad C_L = \frac{2 * F_y}{\rho * v^2 * A} \qquad (2.2)$$

Here, C_D is the coefficient of drag and C_L the coefficient of lift while, ρ denotes the density of air at 25°C i.e. 1.184 kg/m^3, v denotes velocity (38.8 m/s), A denotes the chord length of the airfoil for a 2D study. As the airfoil lengths vary marginally, the Reynolds number for this study is equivalent to $\approx 695,000$.

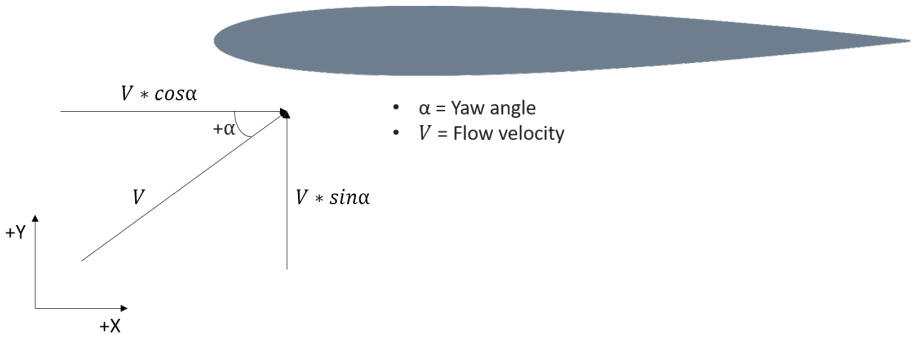

Figure 2.2: *Coordinate system used for 2D studies*

2.1.2 Solver and flow parameters

The simulations were performed using Reynolds-Averaged Navier Stokes (RANS) solver. SST K-Omega Turbulence model developed by F. Menter[13] was used in this study. Incompressible flow was assumed since the flow velocity does not exceed Mach 0.3. Flow velocity of the air was set to $140Km/h$ or $38.89m/s$ as asked by Automobili Lamborghini S.p.A. For the positive yaw sweeps, the flow inlet and the bottom of the domain were set as the velocity inlets, while the top of the domain and flow outlet of the domain were set as the pressure outlets. For negative yaw sweeps, the flow inlet and the top of the domain were set as the velocity inlet, the bottom of the domain and the flow outlet of the domain were set as the pressure outlet.

2.2 Mesh Study

Mesh study is a process of checking the dependency of the solutions based on the refinement in mesh cell size. This study aims to find a mesh with sufficiently high accuracy while keeping the computational cost low. In the earlier phase of the thesis, it was decided to keep the airfoil's position in the domain fixed and vary the direction of the fluid (in this case air) to achieve the yaw changes. This helps in avoiding re-meshing by keeping the same mesh constraints for all yaw angles. Polyhedral mesher was used. To capture the viscous boundary layer, All Y+ Wall Treatment was used and Y+ values were maintained between 1 to 5. To achieve this, the number of prism layers were set to 13 and the thickness of the prism layers to be 2mm, this can be seen in Figure 2.3. To capture a better flow resolution, multiple refinement regions were introduced; near-airfoil offset region, trailing edge refinement, near-wake refinement region and farther wake refinement region. These refinement regions can be observed in Figure 2.4.

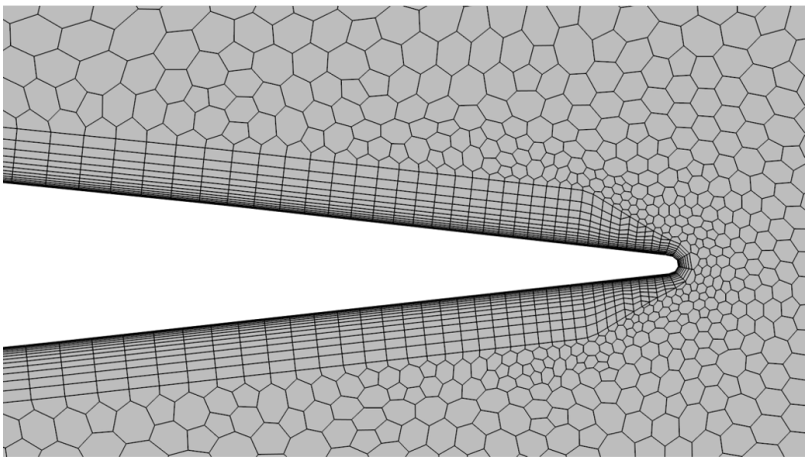

Figure 2.3: *Prism layers near the airfoil*

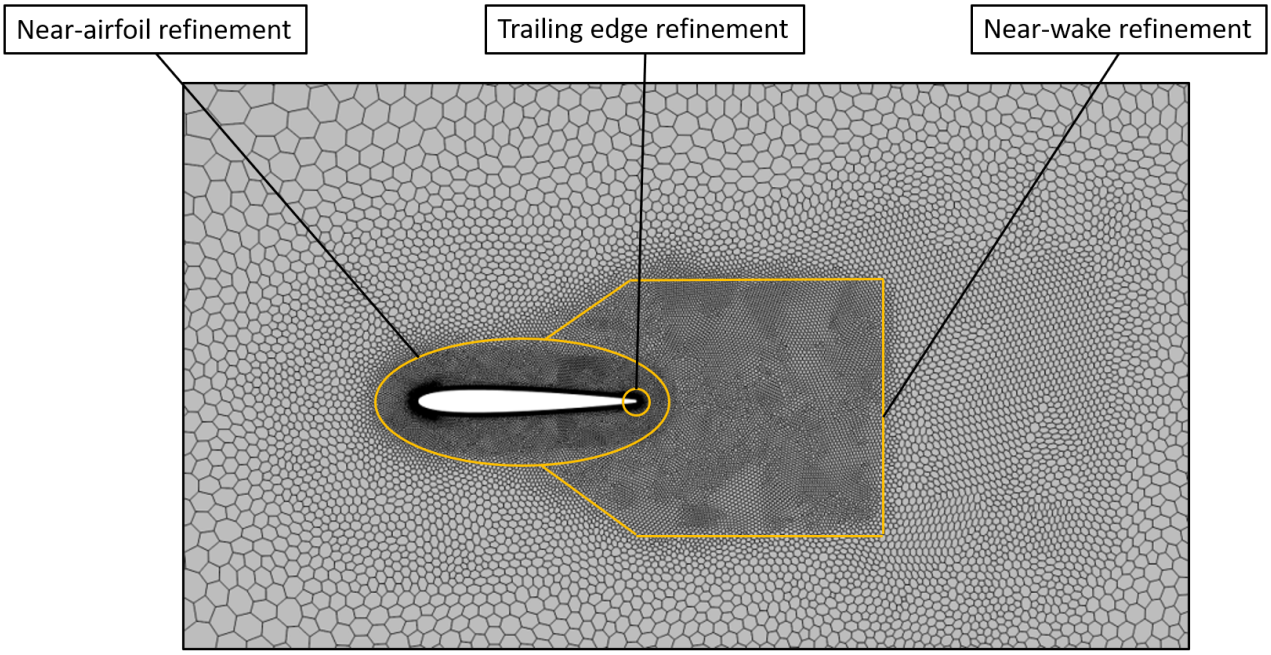

Figure 2.4: *Refinement regions around the airfoil*

A mesh independence study was carried out on the NACA0010 airfoil to ensure that the results were not influenced by the current mesh settings. Figure 2.5 shows the drag coefficient for 0° yaw and lift coefficient for 12.5° yaw, for varying meshes. As 15° yaw angle resulted in completely detached flow, it was better to perform lift analysis on 12.5° yaw angle instead. The smallest cell size tested was $1.75mm$. It was observed that increasing the number of cells beyond 3mm base size did not result in significant changes for either case. Thus, 3mm base size ($\approx 80k$ cells) was used for all the simulations in 2D study. The surface cells on the airfoil were half of the base size.

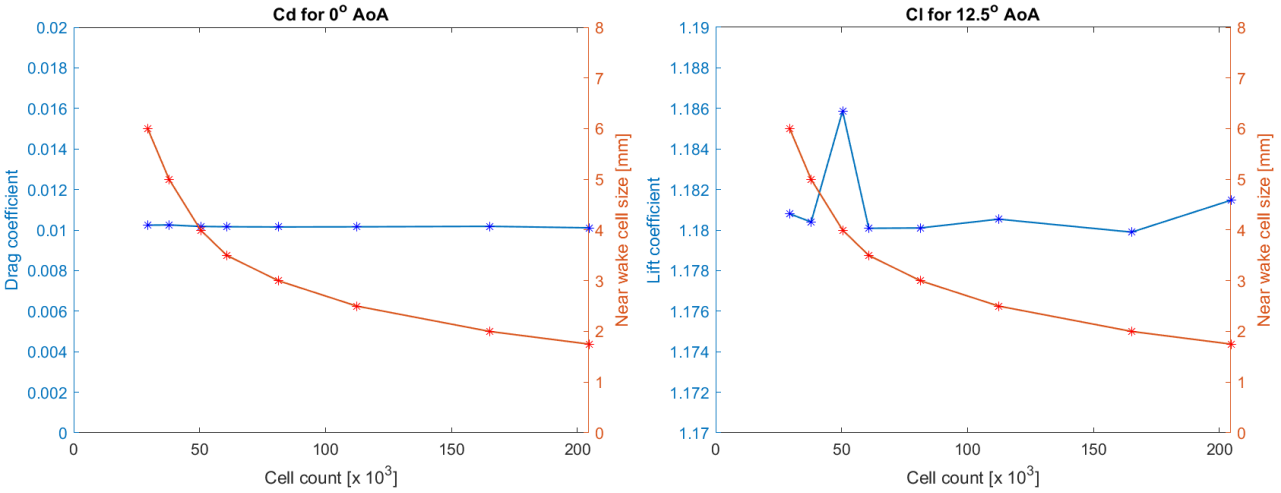

(a) *Coefficient of drag at* 0∘ *yaw*

(b) *Coefficient of lift at* 12.5° *yaw*

Figure 2.5: *Mesh independence study performed on NACA0010 airfoil*

2.3 Airfoil Optimization

In the earliest stage of the thesis, it was concluded to set the NACA0010 airfoil as the baseline for the development of other airfoil profiles. This decision was based on the low drag performance at lower yaw angles, as studied in a previous thesis[5]. The NACA0010 profile was obtained from Airfoil Tools (2021)[10]. A

surrogate-based optimizer tool created by Magnus Urquhart[14] using the programming language Julia[15] was utilized to optimize the airfoil profiles. The optimizer works on the principle of minimizing the target value. As this study was for a dual pylon approach, the average of absolute lift values generated at $+7.5°$ and $-7.5°$ were maximized (negative lift values were minimized). This condition was selected so that a balance between low drag and high lift can be achieved at $0°$ and $15°$ yaw angles respectively.

The optimization was performed by running a Julia script that had an embedded MATLAB code to generate airfoils based on various parameters. This code utilized the IGP[16] function that uses nine variables to generate data points for the corresponding airfoil. Out of the nine parameters, eight were airfoil design parameters while the remaining one defined the resolution of data points which was set to 300. These airfoils were given an additional parameter, rotation concerning the global coordinates. Thus, a total of nine parameters were defining the range of optimization and this can be seen in Table 2.1.

Parameter		**Range**
Global Rotation		-2.5 to +2.5
Camber line abscissa coefficient	c1	0 to 2
	c2	0 to 2
Camber line ordinate coefficient	c3	0 to 1
	c4	0 to 0.3
Maximum thickness		0.05 to 0.3
Maximum thickness position		0.1 to 0.3
Relative leading edge radius		0.2 to 4
Relative trailing edge radius		0.5 to 4

Table 2.1: Ranges for parameters defining the airfoil

2.4 Passive and Active Systems

The thesis aims to improve the performance of the airfoils at yaw angles of up to $15°$ both in +ve and -ve yaw conditions. Tests were conducted to study the performance of the generated airfoils for an array of yaw angles up to $15°$. To tackle separation occurring at higher yaw angles, passive and active systems were implemented on the airfoil to attach the flow.

2.4.1 Passive system

The passive system is implemented using the slotted design of airfoils as seen in Figure 2.6a. The slot guides the air from one side in order to attach the flow on the other side. However, this approach comes with the penalty of disturbing the flow in other direction. Thus, the optimized airfoils were vital in considering this approach. The optimum slot for a profile was decided by the highest average lift values at $\pm 15°$ yaw angle. A dual (cross) slot system was previously explored in the thesis[5] that preceded this. Dual slot was incapable of providing attached flow in either direction at higher yaw angles. The single slot approach aimed at improving the flow on one side of the pylon, and would be focused at improving performance over the inner wheel while cornering. Thus, a single slot approach better suited the purpose of this thesis.

2.4.2 Active system

The active system implemented was basically a flow control method, either by blowing the flow tangential to the airfoil surface using a slot, or by creating a suction normal into the airfoil using a notch. These methods solve the problem of detached flow at higher yaw angles. For the blowing method, a stagnation inlet was used to mimic the ALA system[2]. Using a $3mm$ slot, the stagnation inlet was set at $533Pa$ based on a fraction of the flow speed. This condition was fixed for the blowing method as any slot below $3mm$ would be difficult to manufacture, while a larger slot would disturb the flow further, especially when it is inactive. Also, an increased slot would have a reduced flow speed as a similar flow rate was to be maintained. This active slot was tested across various positions along the chord length for each profile to ensure optimum performance. An example of the active blowing approach is shown in Figure 2.6b, where the wind annotation signifies the blowing slot in +X direction.

The idea behind alternative active approach, motorized suction, was to expend energy in order to create a suction that maintained a constant flow rate. This was implemented using a negative velocity inlet on the notch created over the airfoil surface (shown in Figure 3.6). With efficiency in question, this method was only implemented when the blowing method was ineffective. For suction, the velocity could be varied as it is controlled, but it was important to consider power consumption for the ideal design. This method also results in complex construction and manufacturing of parts. These limitations can offset the purpose of the active systems to improve the car's aerodynamic performance. However, with a notch design, the airfoil would not undergo a significant redesign, unlike a slot for active blowing. Thus, it can be placed before the point maximum thickness, which makes it effective on designs that have detached flow right at the leading edge.

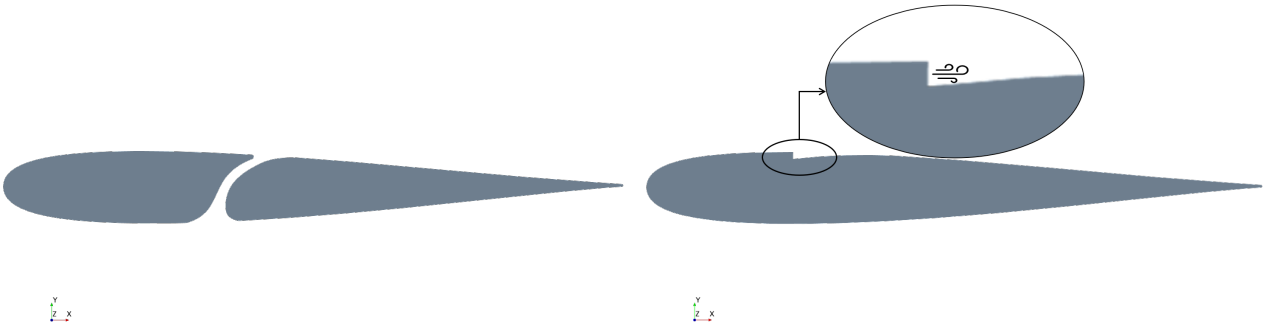

(a) *Passive* (b) *Active*

Figure 2.6: *Example of an airfoil with passive and active systems*

3 Results & Discussion - Airfoil Study

In this section, the generated airfoils and results of the airfoil performance will be presented in steps starting from NACA0010 which was considered as the base profile. Other generated airfoil profiles will follow after presenting the base profile. The sweep study is performed in intervals of 1° between 0° and 5°, while the interval increases to 2.5° between 5° and 15° yaw angles.

3.1 Generated Airfoils

The range of parameters defined in Table 2.1 were used by the surrogate model to test out various airfoils. With freedom to generate asymmetric airfoils, the surrogate model varied the parameters in order to arrive at profiles with best lift capabilities at ±7.5° yaw. Figure 3.1 shows a cluster of airfoils generated by the optimizer. The generated airfoils were simulated in STAR-CCM+ for both the angles.

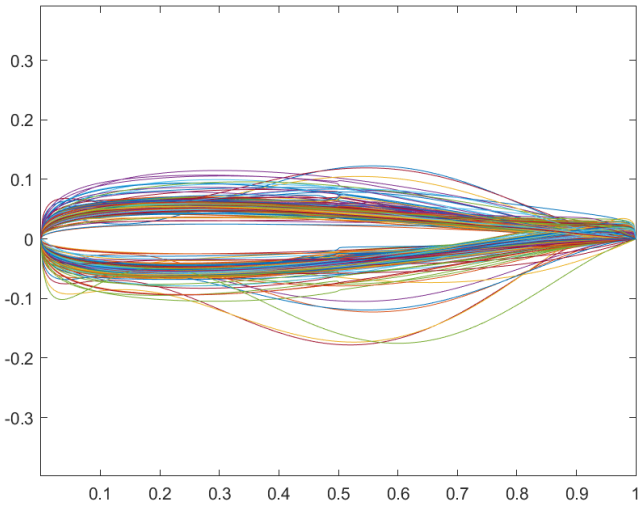

Figure 3.1: *Airfoils generated by optimizer using IGP*

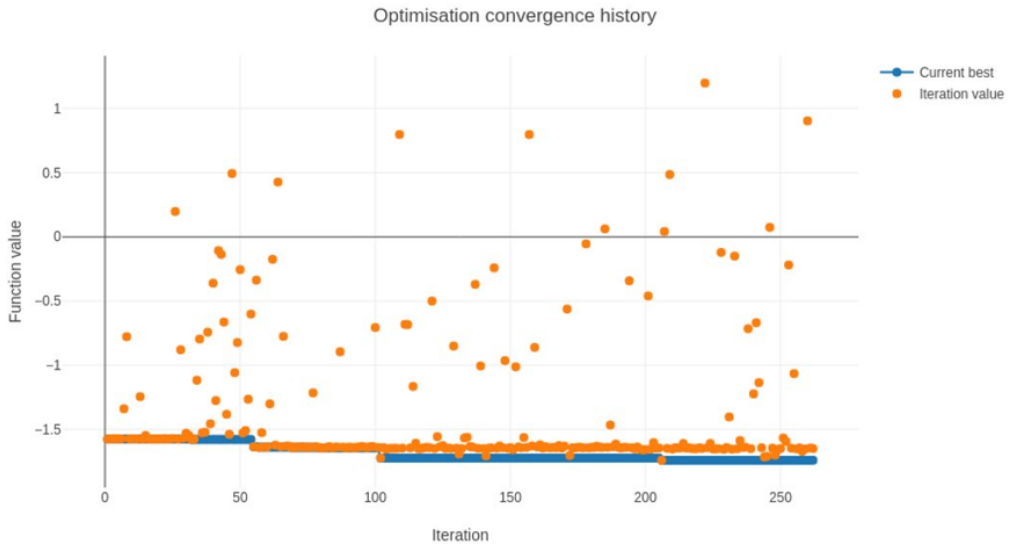

Figure 3.2: *Julia optimisation history*

Figure 3.2 shows an example of how the optimizer iterated to achieve maximum lift. The Y axis denotes the summation of negative lift values at ±7.5° yaw. The orange dots resemble the lift values at a specific iteration.

The optimizer ran for many such loops which generated numerous profiles and were tested in STAR-CCM+ until the lift values saw insignificant improvements and the parameters defining the airfoils started to saturate. As the parameter range was wide, some of the generated airfoils performed badly. These outliers can be evidently seen in Figures 3.1 and 3.2. Some airfoils generated were self intersecting as well and could not be simulated in STAR-CCM+.

After running the optimizer a couple of times, three airfoils were selected based on their performances. The parameters defining these airfoils can be seen in Table 3.1. Both abscissa coefficients were capped at 1 for Case 1. All three cases have different thicknesses and were arranged in an increasing order. Between Case 2 and Case 3, all parameters except maximum thickness were quite similar. All parameters other than the trailing edge radius were well within the defined ranges. Thus, they are not bounded by the range. It was interesting to see how the optimizer focused on making the trailing edge thinner. Manufacturing constraints needed to be considered, thus 0.5 was set as the minimum limit.

Parameters		**Airfoils**		
		Case 1	**Case 2**	**Case 2**
Global Rotation		-0.38	-0.58	-0.36
Camber line abscissa coefficient	c1	1.00	1.69	1.73
	c2	1.00	1.09	1.09
Camber line ordinate coefficient	c3	0	0	0
	c4	0.02	0.04	0.04
Maximum thickness		0.11	0.13	0.15
Maximum thickness position		0.23	0.26	0.26
Relative leading edge radius		0.50	0.59	0.57
Relative trailing edge radius		0.79	0.50	0.50

Table 3.1: Parameters defining the airfoil

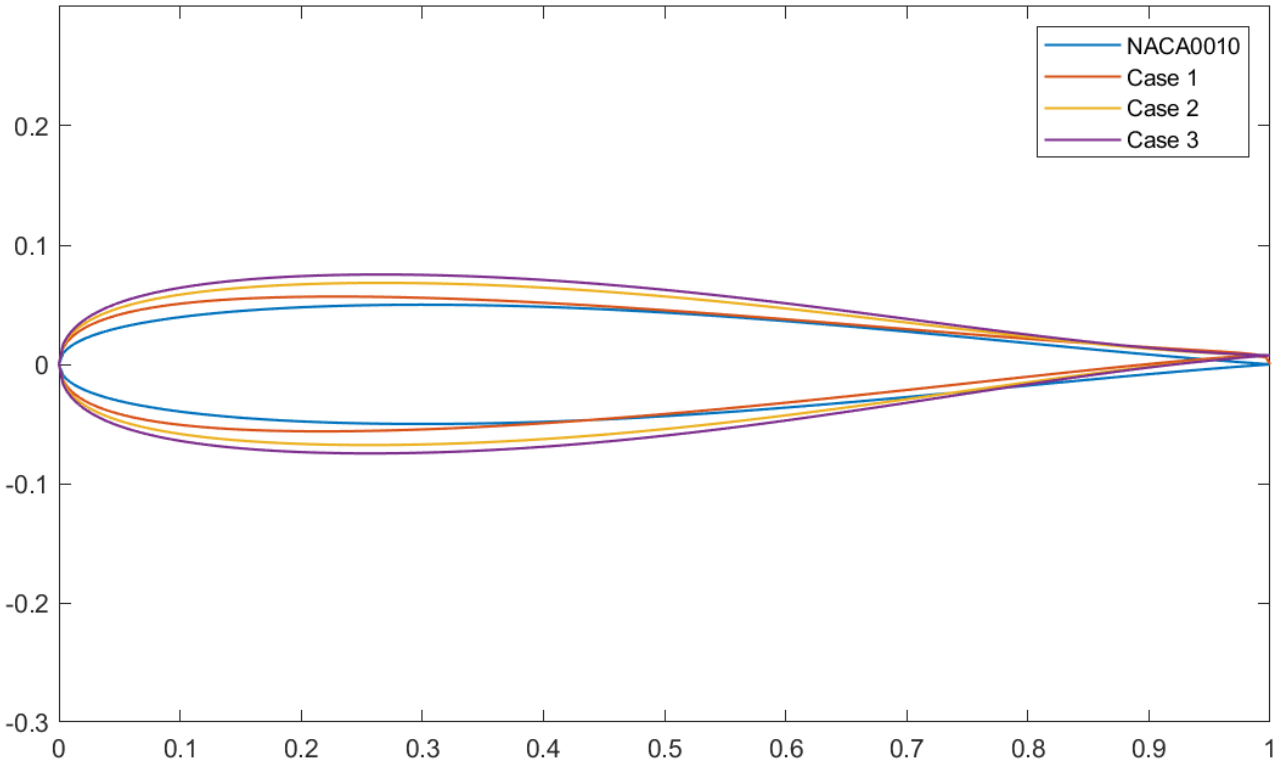

Figure 3.3: *Airfoils selected for the study*

Figure 3.3 represents the three best designs which were selected from the generated lot of profiles. The selection

was based on the airfoil performances at low and high yaw angles. It can be observed that thicknesses of the selected airfoils are larger than the NACA0010 profile, as it helps accelerate flow around the leading edge at greater yaw angles. The global rotation was not included in the airfoil plots. This was implemented when the airfoils were imported in STAR-CCM+, where it was also ensured that none of the airfoils had a trailing edge thickness lesser than $1mm$.

3.2 NACA0010

Yaw sweep was performed on the NACA0010 airfoil at 140Km/h and the following results were obtained. Since the airfoil is symmetric, only positive yaw results are shown. The sweep study shows that the NACA0010 airfoil keeps the flow attached till 12.5° yaw and detaches at 15° yaw. This can be seen from Figure 3.5. Being a thin airfoil, NACA0010 had the lowest drag amongst other airfoils studied in the previous thesis[5]. However, that results in a lower robustness against high yaw angles.

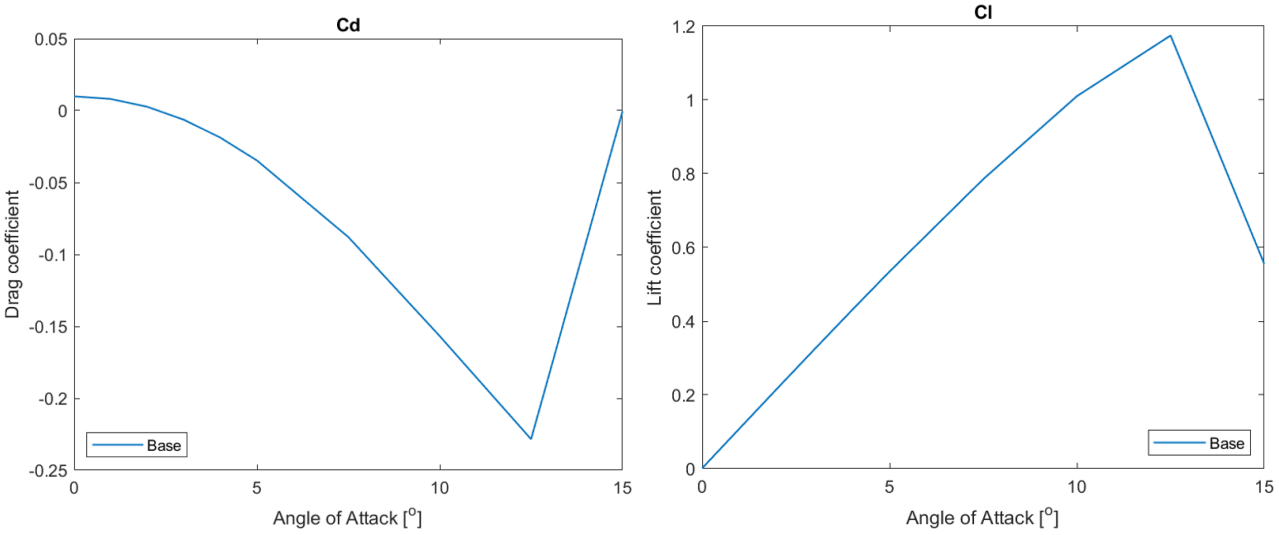

(a) *Coefficient of drag* (b) *Coefficient of lift*

Figure 3.4: *NACA0010 yaw sweep results*

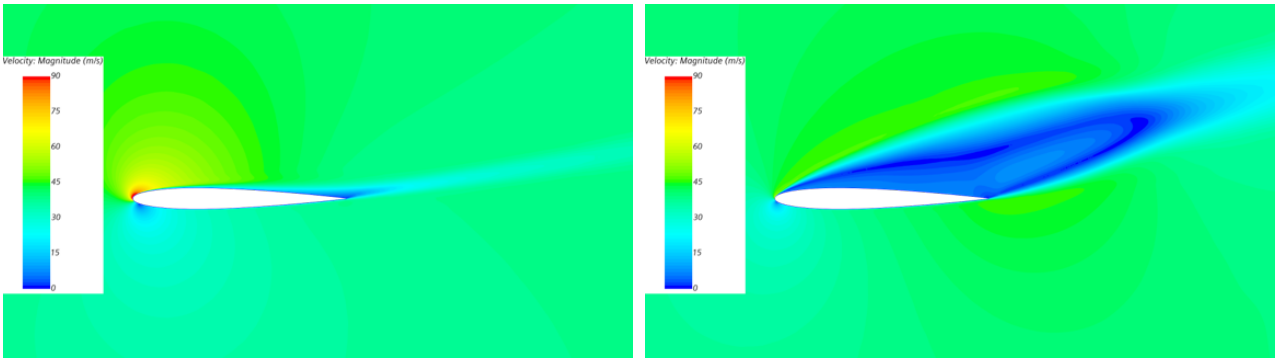

(a) *12.5° yaw* (b) *15° yaw*

Figure 3.5: *NACA0010 yaw sweep velocity distribution*

Implementing a passive system is not suitable for NACA0010 as it has a completely detached flow for ±15°. Attached flow on one side could be observed by adding a slot, however, the opposite flow was ruined for middle yaw angles too. Passive system for NACA0010 was not included in this study as it was not an optimal result.

3.2.1 NACA0010: Active

Earlier the separation occurs, the greater is the demand from the active system to pull in the entire airflow. With a stagnation inlet approach, a high velocity could not be achieved, thus the blowing approach could not be placed closer to the leading edge as that region needs to have high accelerated flow for attachment. Hence, the active system was placed further back along the chord length. After testing out all positions along the chord length, this approach was discarded. The other active method in our project scope was to provide a motorized suction. To simulate this system, a constant negative velocity inlet was introduced over the body of the airfoil as seen in Figure 3.6. With this approach, attached flow could be achieved for $+15°$ yaw, while the $-15°$ case would still have detached flow.

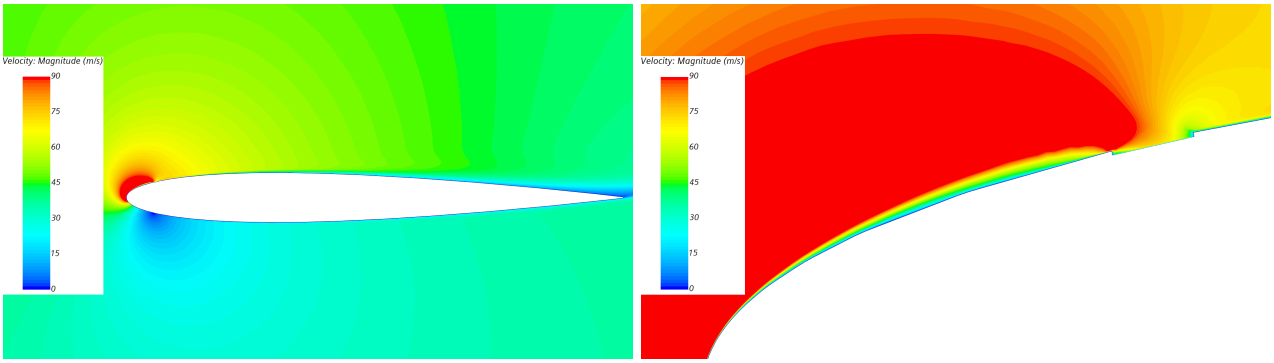

(a) *Flow with suction active at* $+15°$ *yaw* (b) *Close up on the notch at* $+15°$ *yaw*

Figure 3.6: *Velocity scalar scene for NACA0010 with a 3mm wide notch placed at 5% chord length*

With a maximum suction of $30m/s$ available, a sensitivity analysis was conducted to find the optimum position and suction velocity as seen in Figure 3.7a. Even though the maximum speed was defined, $35m/s$ was tested to see the saturating trend of results. Speeds below $30m/s$ at 10% chord length were struggling to keep the flow attached, and did not work at all below $20m/s$. From this study, it was concluded that a suction at 7.5% chord length with speed on $25m/s$ is optimum. A sweep study was performed on all these combinations, and as seen in Figure 3.7b, the boost in performance is immense beyond $+12.5°$ yaw.

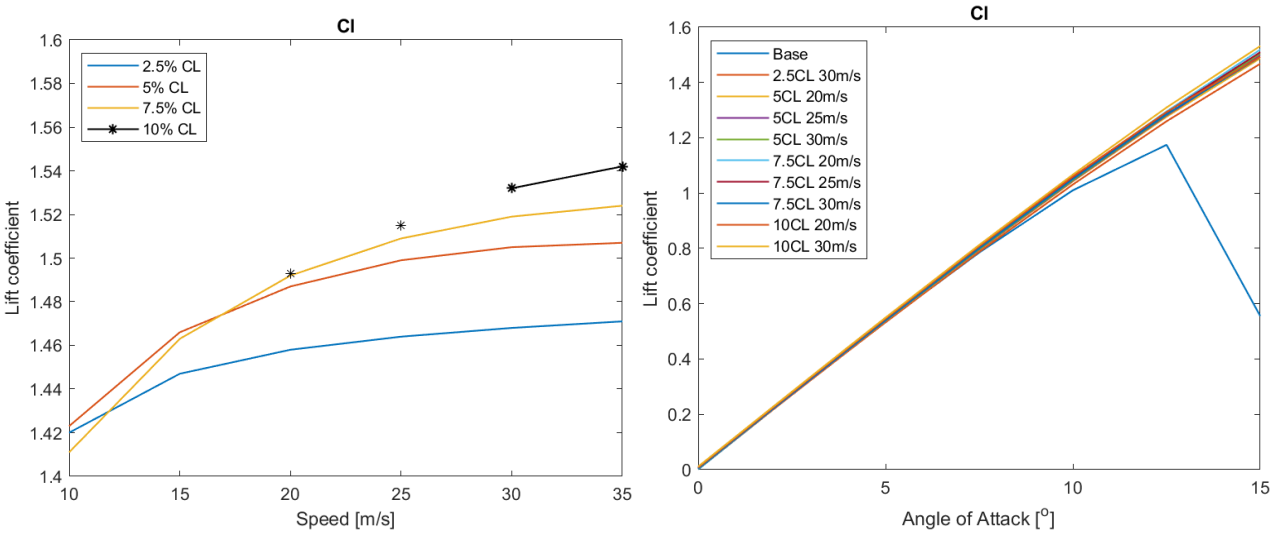

(a) *Sensitivity to position and suction speed at* $+15°$ *yaw* (b) *Positive sweep study on the various active configurations*

Figure 3.7: *Lift coefficients for NACA0010 with active suction*

3.3 Case 1

The earlier NACA0010 airfoil was a symmetric profile. The Case 1 airfoil is an asymmetric profile along with $-0.4°$ rotation. The airfoil generated also has a maximum thickness greater than the NACA0010 profile. The flow attachment at higher yaw condition can be observed from Figure 3.9b. However, the $+15°$ yaw still has flow detachment. This can be improved by the passive and active systems as mentioned earlier. As the negative yaw rotation of the airfoil helps the flow to stay attached for a bit longer in the negative yaw side of the airfoil, passive system can be used to aid the positive air flow. It is to be noted that the graphs contain both yaw conditions in the same axes. The negative yaw results, in actuality have the opposite sign to that of the positive yaw results. To make the comparison easier, both conditions were represented in the same graph by keeping the same sign convention. Overall, when the positive and negative yaw lift values were averaged, Case 1 outperformed the NACA0010 with a drag penalty of 1 count.

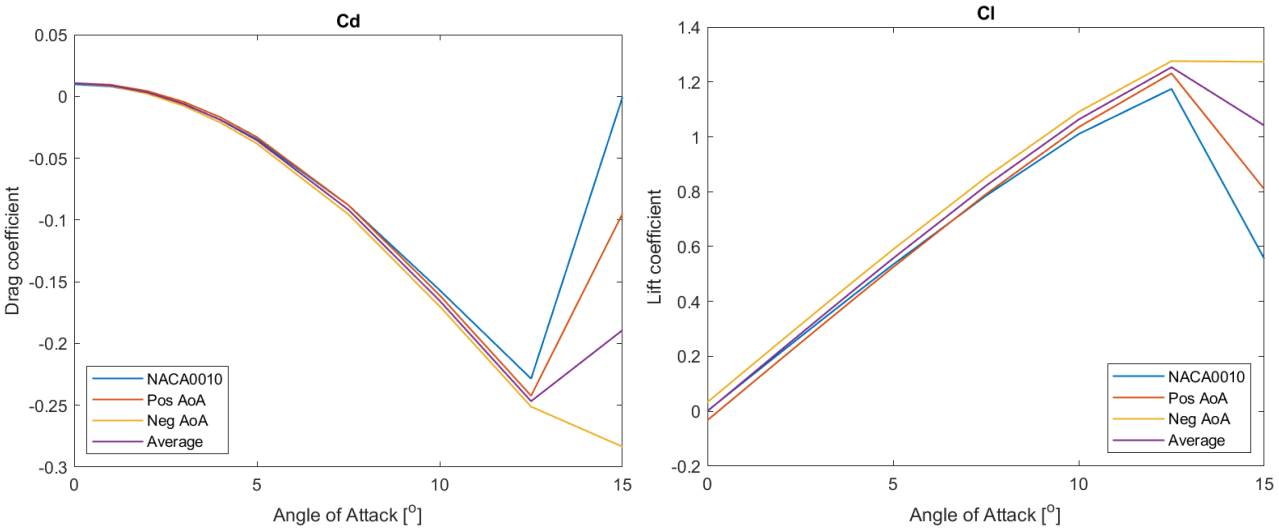

(a) *Coefficient of drag* (b) *Coefficient of lift*

Figure 3.8: *Case 1 yaw sweep results*

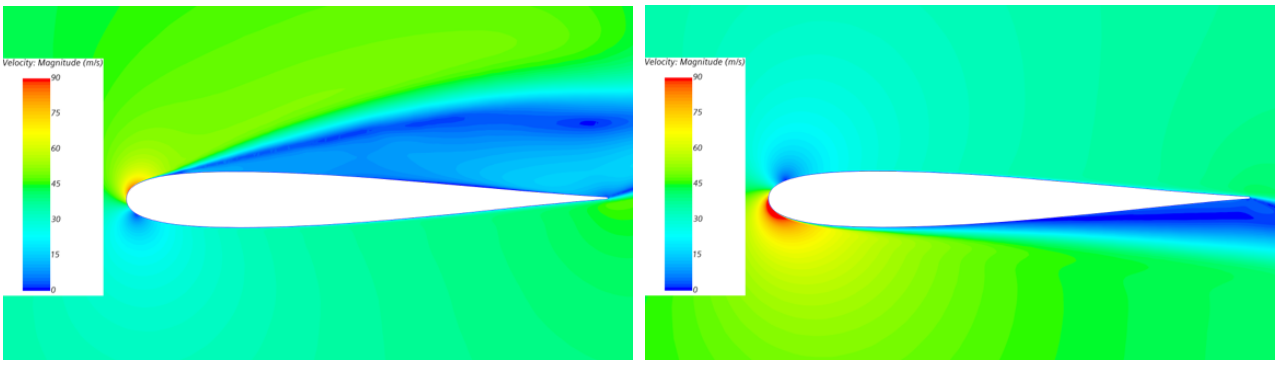

(a) *+15° yaw* (b) *-15° yaw*

Figure 3.9: *Case 1 yaw sweep velocity distribution*

3.3.1 Case 1: Passive

The slot of the passive design was placed at 38% of the chord length, this can be observed in Figure 3.11. The results for the passive system are presented in Figure 3.10. From the graph in Figure 3.10b it can be seen that the passive system at $+15°$ yaw generates a lift of 1.437. In the negative yaw the system generates a lift

of 1.107. The base profile however, has better performance in terms of lift and drag until 12.5° yaw. This is because the passive designs were optimized for +15° yaw conditions. The negative yaw angle performance for this design was not bad, especially at lower yaw angles. The negative separation gradually increases with increasing yaw angle.

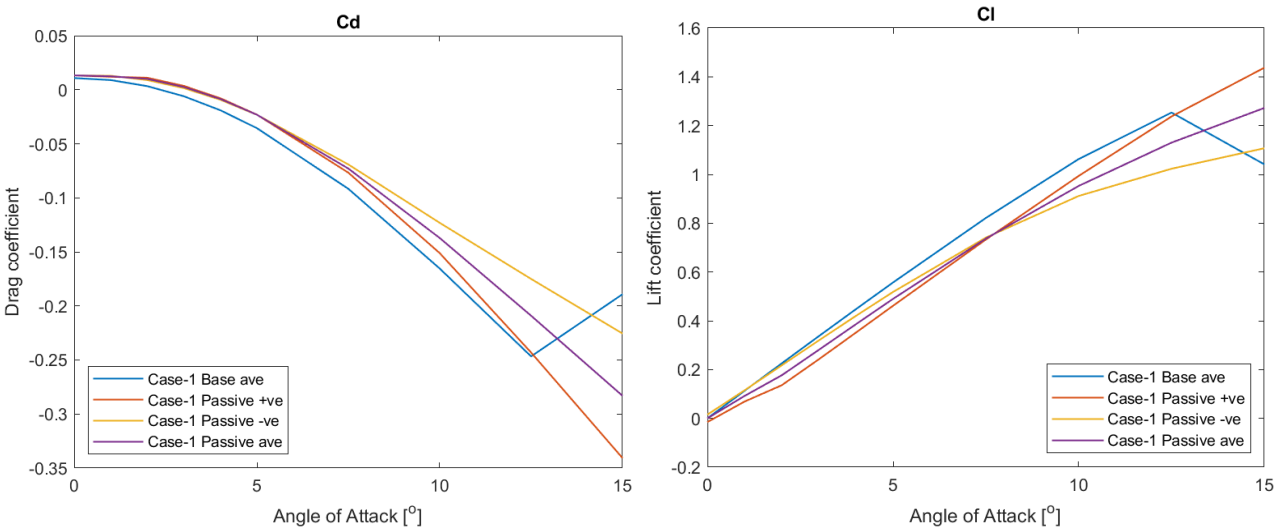

(a) *Coefficient of drag* (b) *Coefficient of lift*

Figure 3.10: *Case 1 yaw sweep results with passive system*

The averaged lift values for the 15° yaw condition for this passive design provides a 1.272 lift. This is better when compared with the base Case 1 airfoil's average lift of 1.213. This highlights the con of passive system. While it increases performance at the yaw angle where a closed profile would have a detached flow, its performance is sub-par at angles below detachment angle.

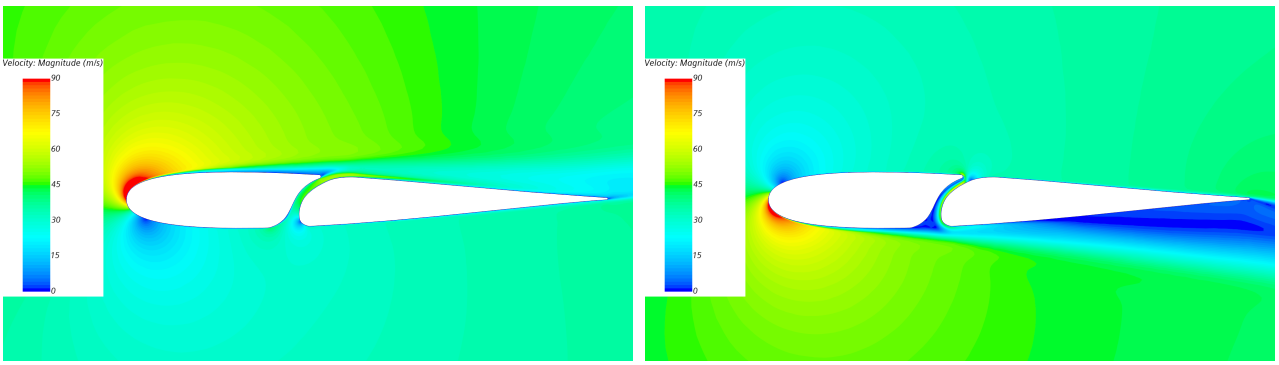

(a) *+15° yaw* (b) *-15° yaw*

Figure 3.11: *Case 1 yaw sweep velocity distribution with passive system*

3.3.2 Case 1: Active

The graphs shown in Figure 3.12 represent the positive yaw results of the active system. The active slot for blowing was placed at 24% chord length position. Since there are no geometry changes in the negative side, the results remained similar to the base Case 1 airfoil's negative yaw performance. The scalar scene shown in Figure 3.13b has a very good flow attachment. It can be seen that the inactive condition performs very similar to the Case 1's base airfoil's performance at angles below +15° yaw. At +15° yaw, the active blowing can be started to improve the performance drastically. Thereby, proving the effectiveness of the active system in this case.

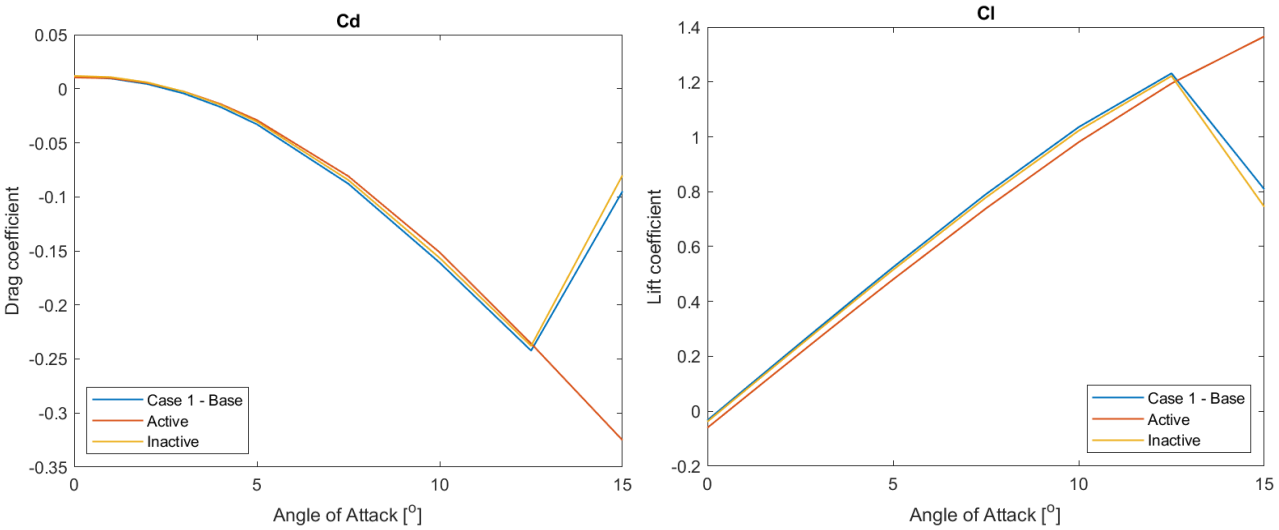

(a) *Coefficient of drag* (b) *Coefficient of lift*

Figure 3.12: *Case 1 yaw sweep results with active system*

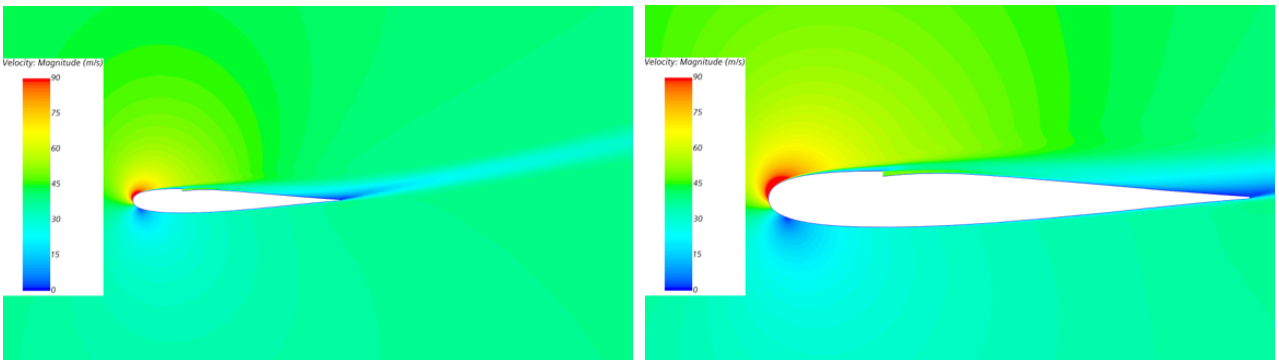

(a) *+15° yaw* (b) *Zoomed in scalar scene*

Figure 3.13: *Case 1 yaw sweep velocity distribution with active system*

3.4 Case 2

Case 2 airfoil is an asymmetric airfoil similar to Case 1 but the differences lie in the rotation and thickness of the profile. Case 2 is slightly thicker and has $-0.58°$ rotation. As seen from Figure 3.14, Case 2 performs better than NACA0010 at higher yaw angles, while facing a drag increment of 2 counts at 0° yaw angle. Unlike Case 1, Case 2 results in decent flow attachment even at $\pm 15°$ yaw angle.

After an iterative process, the Case 2 design was rotated by $-1°$ instead of $-0.58°$. With this change, the C_L at $-15°$ yaw angle increased by 5 counts, however the $+15°$ yaw angle C_L reduced by 29 counts. This was done in order to improve the utilisation of passive and active systems as they would be implemented to improve positive yaw flow. The updated results can be seen in Figure 3.16. It was observed that the average value at 15° yaw has dropped with this tweak, and there was a greater disparity between the positive and negative sweep results. The tweaked configuration ($-1°$ rotation) was used for passive and active system implementation.

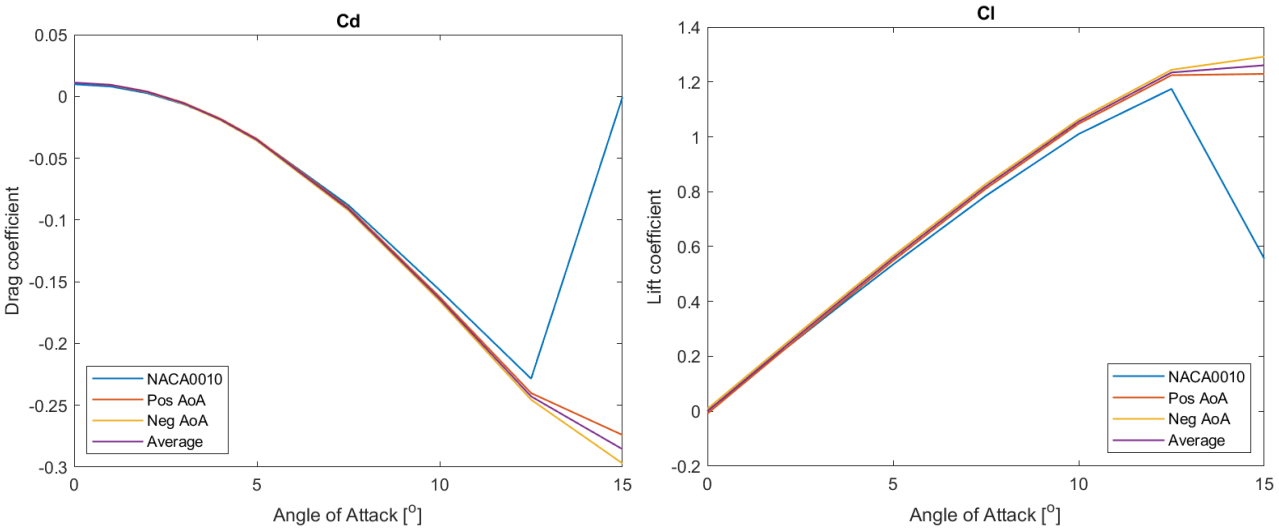

(a) *Coefficient of drag* (b) *Coefficient of lift*

Figure 3.14: *Case 2 yaw sweep results before tweaking*

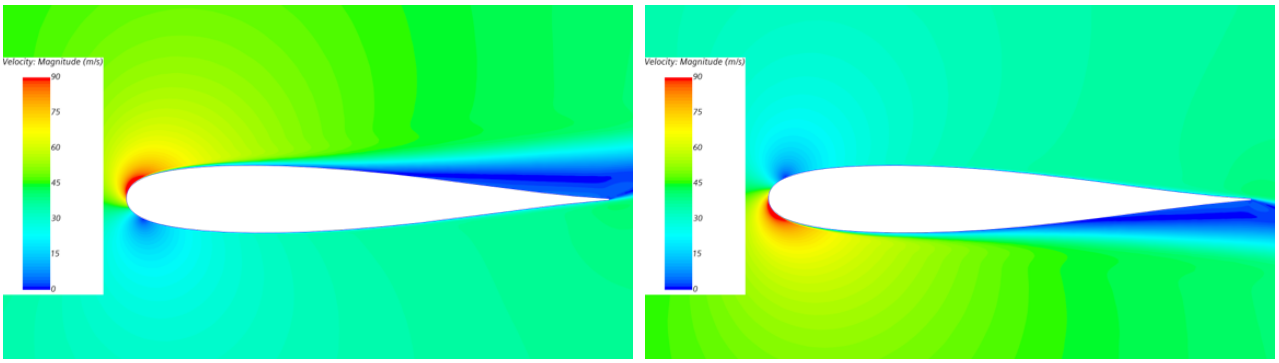

(a) *+15° yaw* (b) *-15° yaw*

Figure 3.15: *Case 2 yaw sweep velocity distribution before tweaking*

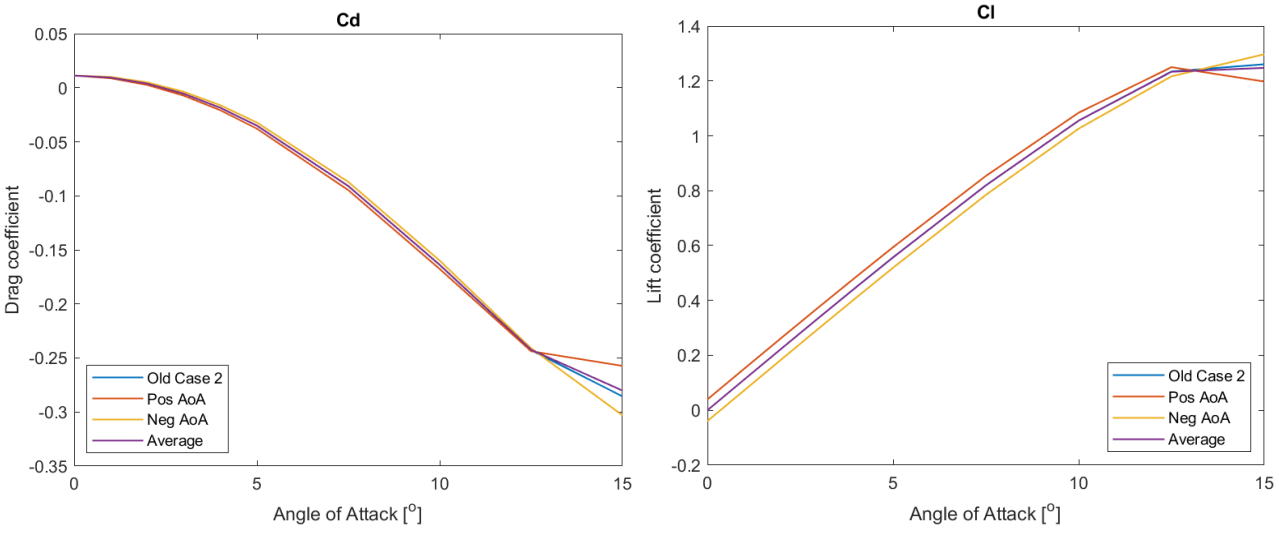

(a) *Coefficient of drag* (b) *Coefficient of lift*

Figure 3.16: *Case 2 yaw sweep results after tweaking*

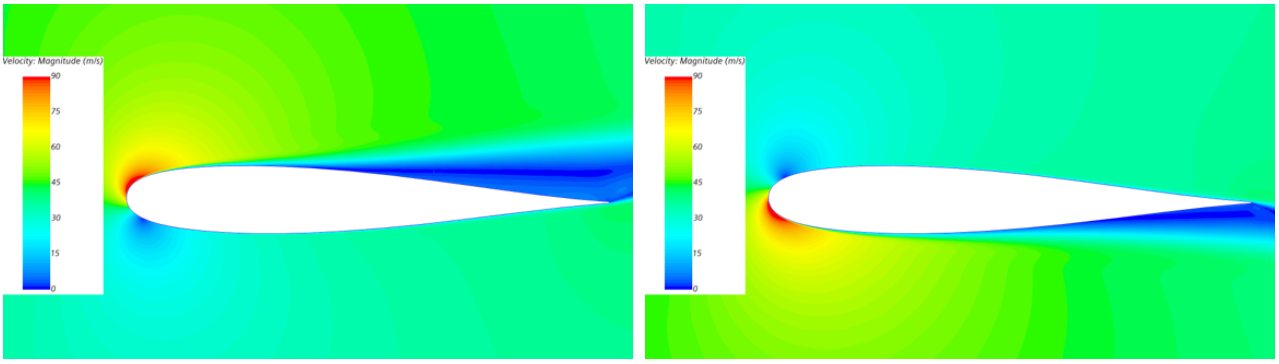

(a) *+15° yaw* (b) *-15° yaw*

Figure 3.17: *Case 2 yaw sweep velocity distribution after tweaking*

3.4.1 Case 2: Passive

The slot for this case was placed at 45% chord length and can be observed in Figure 3.19. When compared with the Case 1's placement of the slot, the slot is pushed further towards the trailing edge of the airfoil. This is due to comparatively delayed detachment of the flow at 15° yaw conditions. Figure 3.18b shows the lift performance of the Case 2 passive design. A maximum lift value of 1.501 can be observed in the +15° yaw, which is much higher than the Case 1's passive system average. However, in −15° yaw, the passive design only provides a lift value of 1.013, this is comparatively lower to Case 1's negative yaw passive system performance. This design fetches a good average performance over the positive and negative yaw sweeps, with a maximum averaged lift value of 1.264. The average lift values of this are better by 17 drag counts when compared to the tweaked (base) Case 2 airfoil's average.

3.4.2 Case 2: Active

The outlet for Case 2's active slot was placed at around 45% chord length similar to the passive system. The positive yaw performance has excellent flow attachment at +15° yaw which can be noticed in Figure 3.21. The difference between the base Case 2 and the inactive performance of this airfoil is very small which can be observed in Figure 3.20b. Thus, once again, the active system can work efficiently by activating only above +10° yaw angle. With good results in negative yaw sweep (same as the base case), this is a very good outcome.

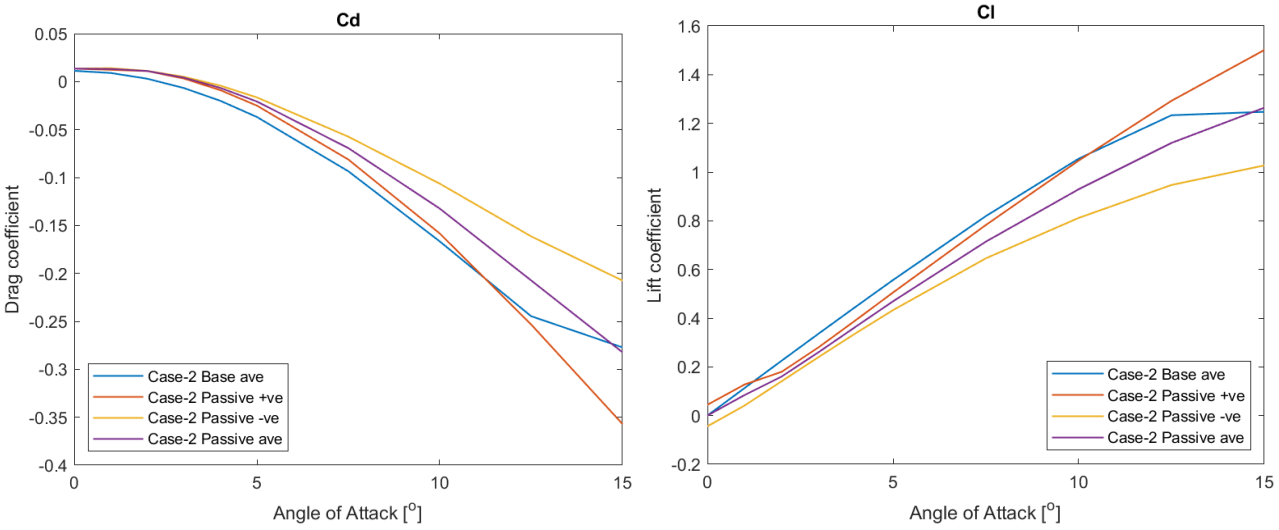

(a) *Coefficient of drag* (b) *Coefficient of lift*

Figure 3.18: *Case 2 yaw sweep results with passive system*

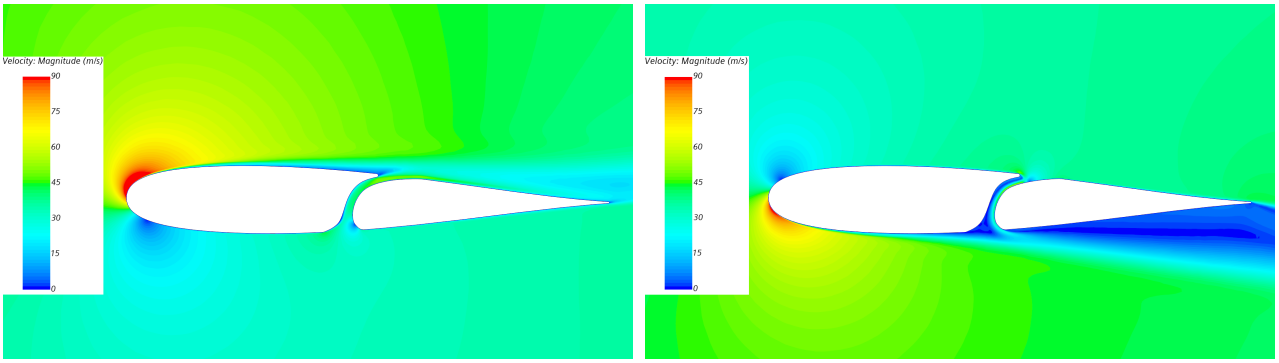

(a) *+15° yaw* (b) *-15° yaw*

Figure 3.19: *Case 2 yaw sweep velocity distribution with passive system*

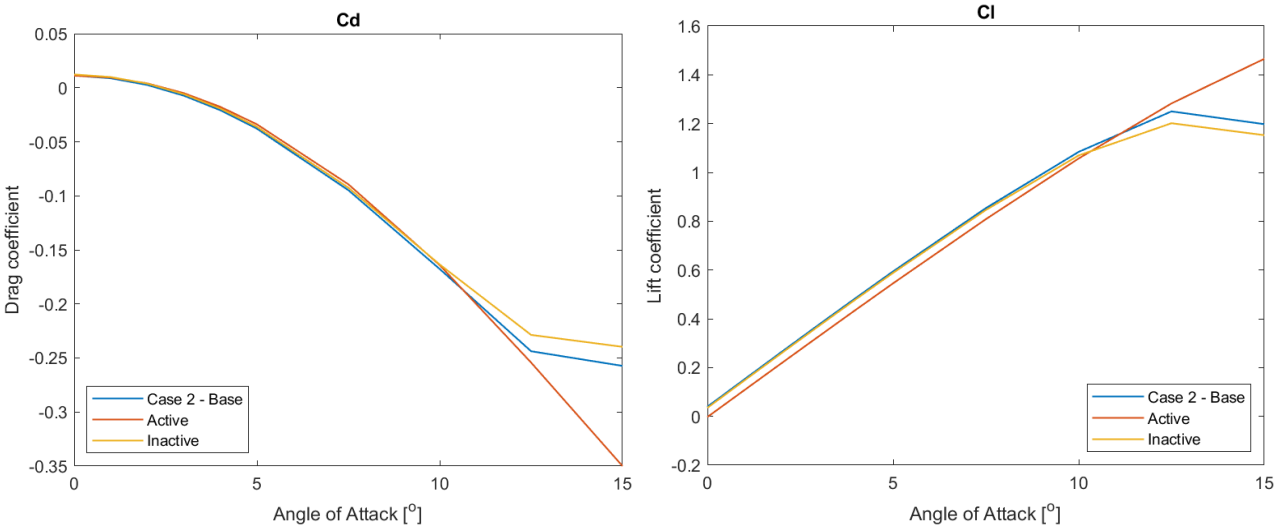

(a) *Coefficient of drag* (b) *Coefficient of lift*

Figure 3.20: *Case 2 yaw sweep results with active system*

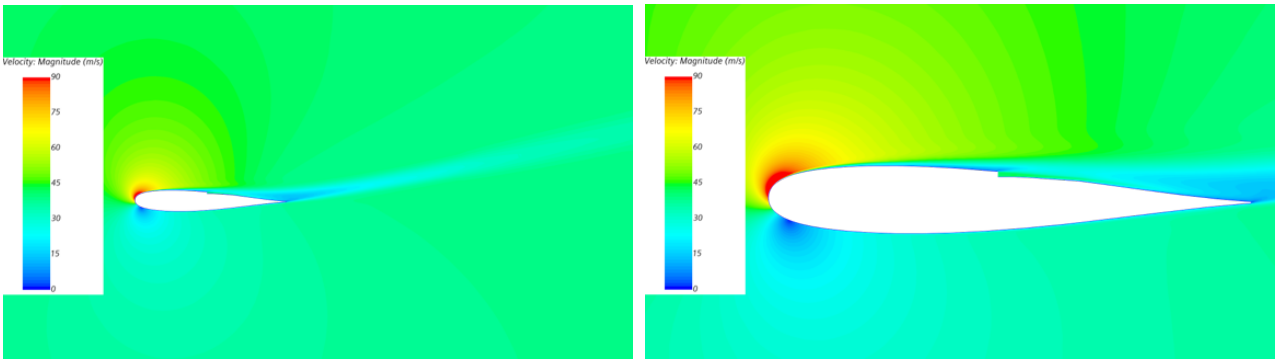

(a) *+15°* (b) *Zoomed in scalar scene*

Figure 3.21: *Case 2 yaw sweep velocity distribution with active system*

3.5 Case 3

The Case 3 profile is the thickest of the airfoils selected and has a rotation of $-0.36°$. The trend for lift coefficient of this case was quite similar to each other at positive and negative yaw conditions shown in Figure 3.22b. Case 3 average C_L always performed better than NACA0010. However, at 0° yaw, Case 3 had 2 counts greater drag. It can be seen that the flow detached a bit later than the Case 2 airfoil's base profile. However, the lift performance did not improve when compared to the Case 2. Their performances were quite similar throughout the sweep as Case 2 performed slightly than Case 3 at 15° yaw.

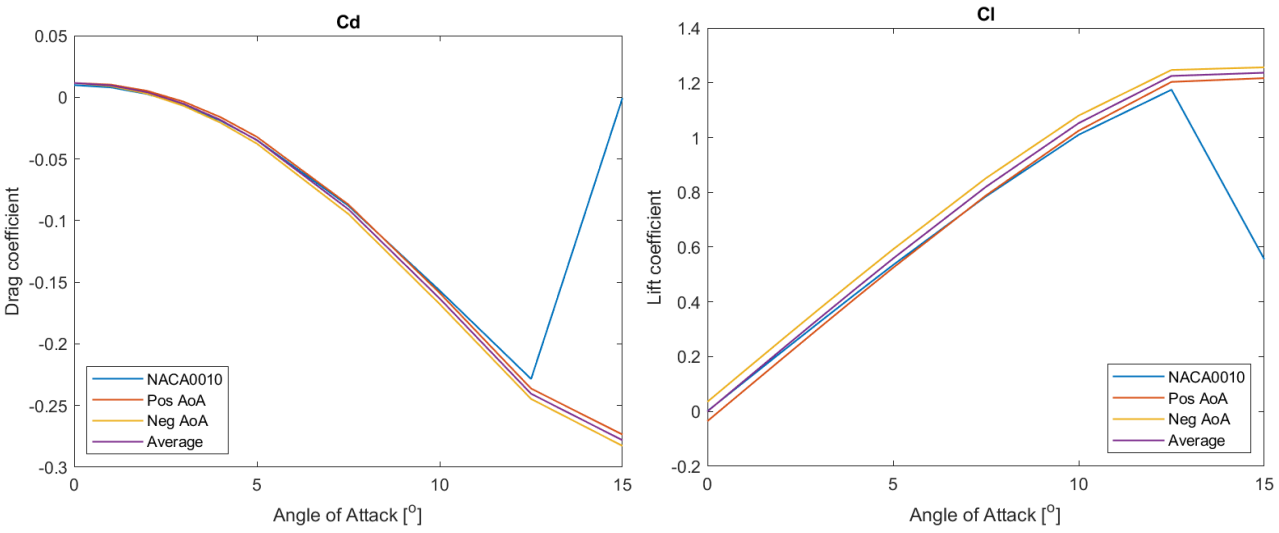

(a) *Coefficient of drag* (b) *Coefficient of lift*

Figure 3.22: *Case 3 yaw sweep results*

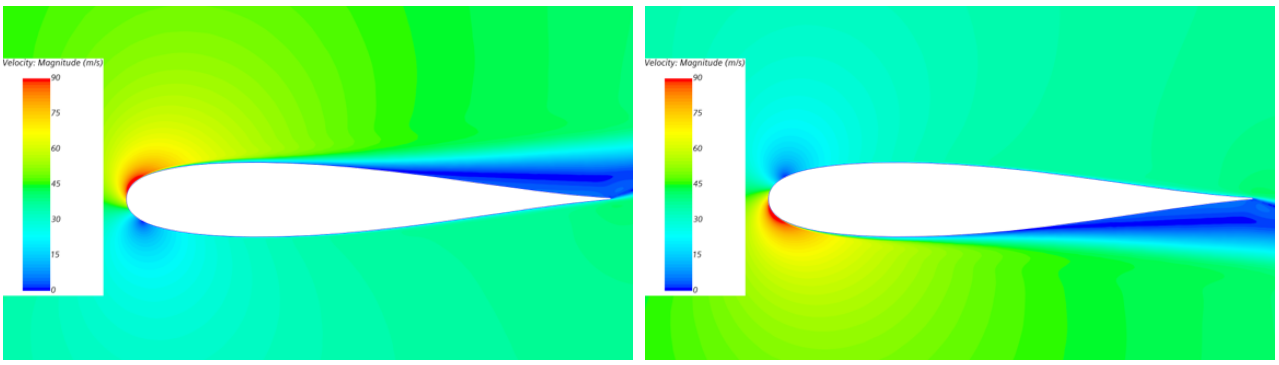

(a) *+15° yaw* (b) *-15° yaw*

Figure 3.23: *Case 3 yaw sweep velocity distribution*

3.5.1 Case 3: Passive

When compared to the passive slot design implemented on the Case 2's airfoil shown in Figure 3.19, the slot for this airfoil is placed further towards the trailing edge at 56% chord length as seen in Figure 3.25. The passive design implemented on this profile fetches a maximum lift value of 1.45 at +15° yaw. At −15° yaw, the passive design has a lift value of 1.05. Overall when averaged both positive and negative yaw performances, the design has a maximum lift value of 1.252, which is better than the closed profile's average of 1.21. However, as seen in the previous two cases, again the lift values of the base profile were better than the passive design at yaw angles below 15°.

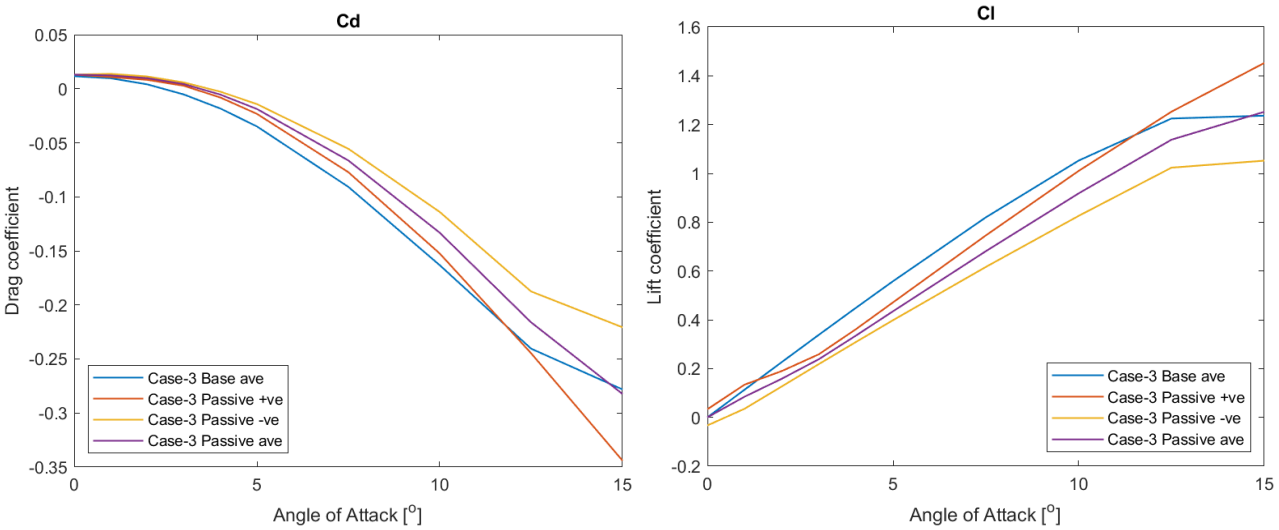

(a) *Coefficient of drag* (b) *Coefficient of lift*

Figure 3.24: *Case 3 yaw sweep results with passive system*

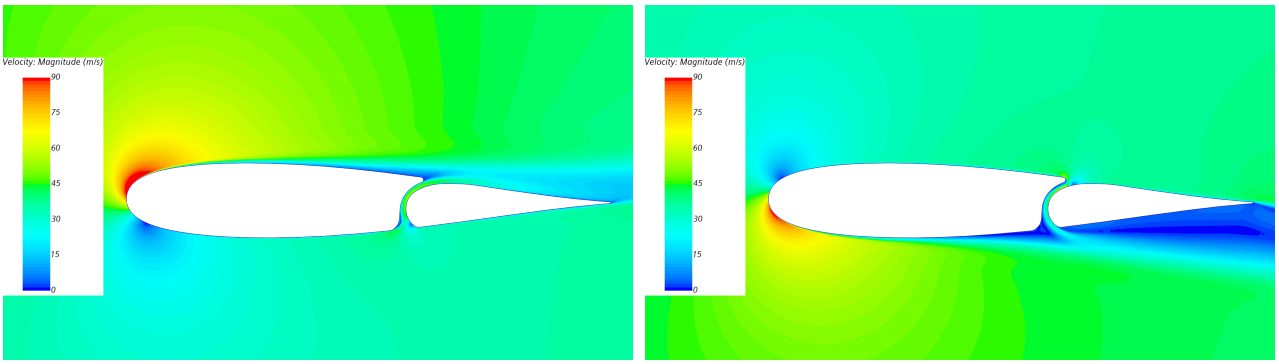

(a) *+15° yaw* (b) *-15° yaw*

Figure 3.25: *Case 3 yaw sweep velocity distribution with passive system*

3.5.2 Case 3: Active

As mentioned in the earlier section, the airfoil has a thicker maximum thickness compared to the other two airfoils. This resulted in a delayed detachment of the flow, this can be seen in Figure 3.27. This lead to the placement of the active outlet comparatively further towards the trailing edge as shown in Figure 3.27b. The active system gave boost in lift performance compared to the base Case 3 profile as seen in 3.26. With inactive condition following the base values closely, active flow is not required until 10° yaw angle.

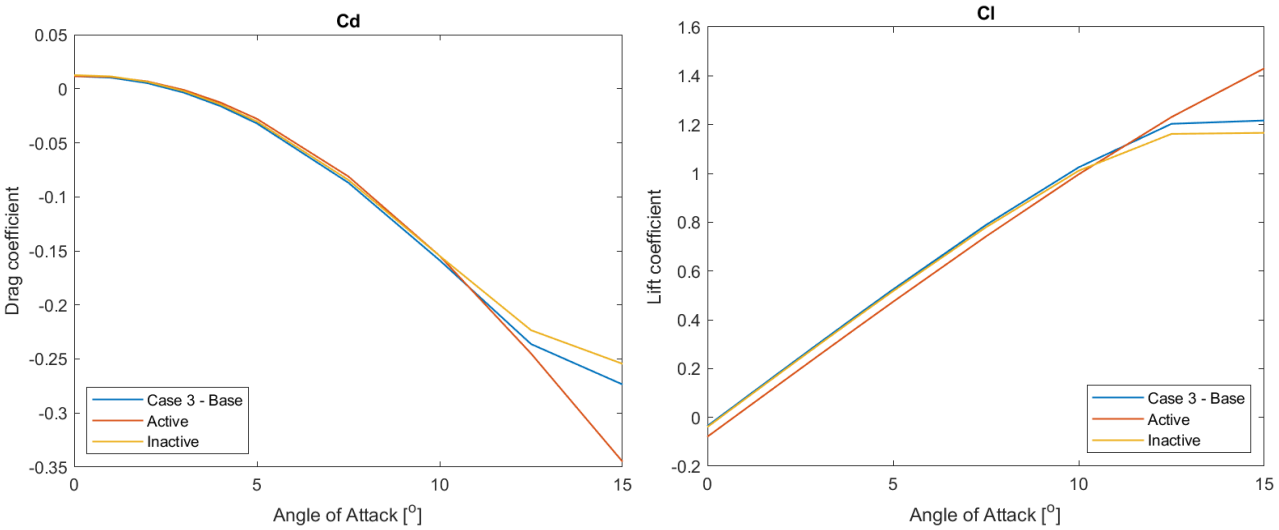

(a) *Coefficient of drag* (b) *Coefficient of lift*

Figure 3.26: *Case 3 yaw sweep results with active system*

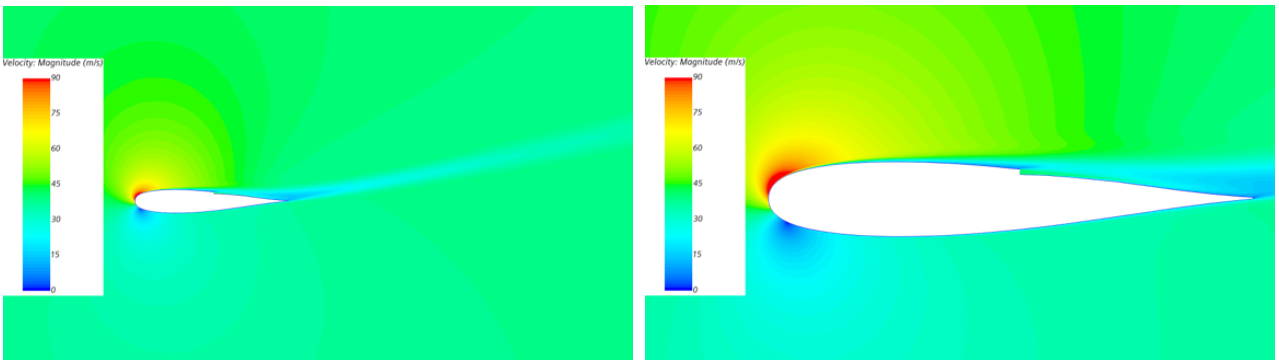

(a) *+15° yaw* (b) *Zoomed in scalar scene*

Figure 3.27: *Case 3 yaw sweep velocity distribution with active system*

3.6 Comparison

In this section, every airfoil's performance will be compared with each other in their respective subsections. While NACA0010 was the best 0° yaw performer, Case 2 was the best performer for 15° yaw.

3.6.1 Closed Profiles

In this section, the generated optimized airfoils will be compared with NACA0010 airfoil. The thicker airfoils maintained a better flow over the surface at higher yaw angles. All of the above-generated profiles were asymmetric in nature bearing a certain amount of yaw rotation. Thus, the average yaw values were considered in Figure 3.28b. It was interesting to see that the asymmetric profiles performed better than the symmetric NACA0010 profile. Case 1 had the highest average lift values until 12.5°, beyond which the flow detached for positive yaw. Thus, it ended up as the worst performer for 15° yaw amongst the generated airfoils. However, its low drag penalty at 0° yaw, along with the potential to generate high lift made it a much better option than NACA0010. Case 2 had the best overall performance in this study. Case 3 however, follows Case 2 with a very similar but minute performance gap in the lift performance. A similar pattern can be observed in the drag performance of the airfoils as well which can be noted from Figure 3.28a.

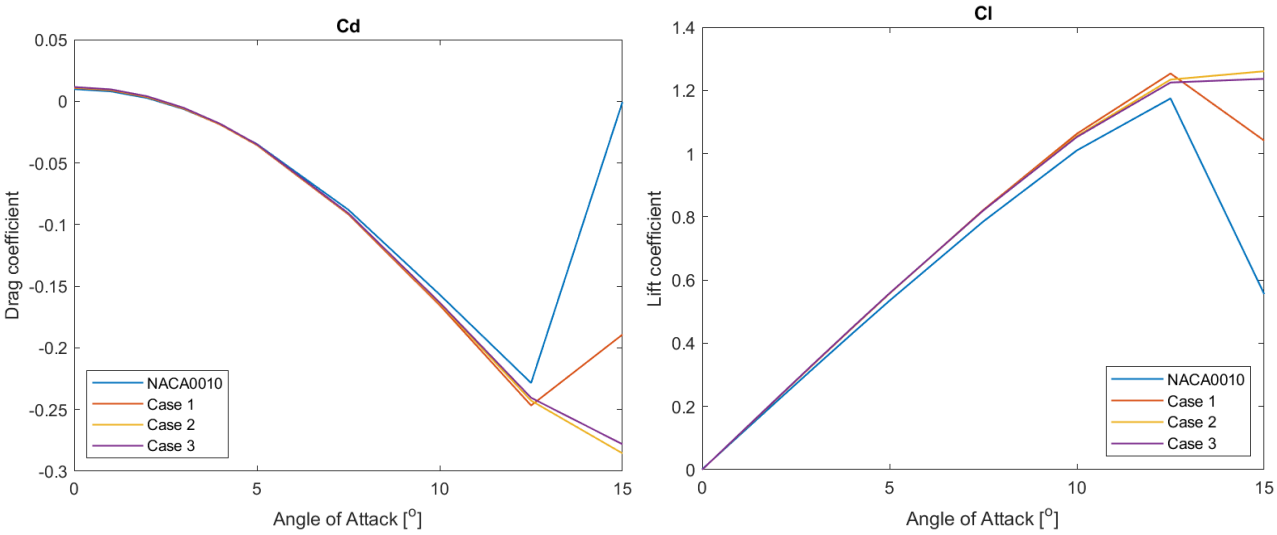

(a) *Coefficient of drag* (b) *Coefficient of lift*

Figure 3.28: *Comparison of the force coefficients for the generated optimized airfoils*

3.6.2 Passive Designs

The passive systems performed better than the respective base profiles only at 15° yaw. However, that is considering the current Reynolds number. When the Reynolds number would decrease, either due to different scaling or change in velocity, the passive systems would have a greater scope of enhancement. The difference in performance between the passive designs were negligible as seen in Figures 3.29 and 3.30. The best performing design in this case was Case 1's passive design, Case 2 being the second best. Case 2 has the best positive yaw performance with a maximum lift value of 1.501 as mentioned earlier. The reason for Case 1's passive design to perform better than the other profiles is because the Case 1 had the highest lift value of 1.103 in −15° yaw condition which resulted in a higher average.

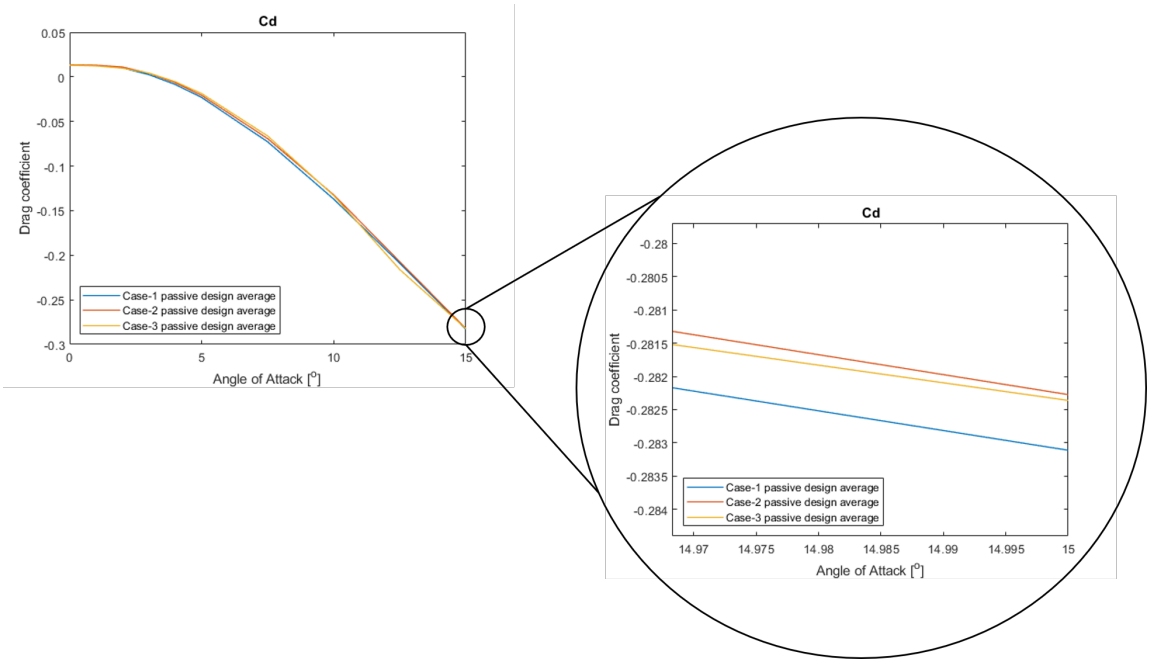

Figure 3.29: *Drag comparison of the generated passive designs*

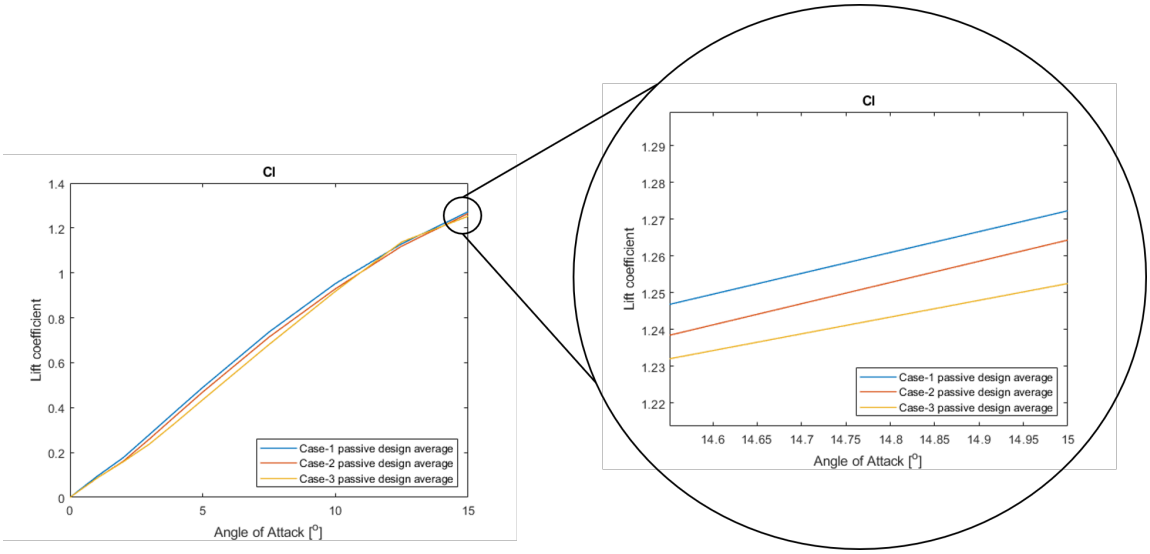

Figure 3.30: *Lift comparison of the generated passive designs*

3.6.3 Active Designs

The lift values of the active cases followed a similar pattern when compared to the base profile cases. In Figure 3.31, only positive yaw results were compared. NACA0010 had the best active performance in terms of drag and lift. However, the active system implemented on NACA0010 was the motorized suction. Lift coefficient of Case 2 performed very similarly to NACA0010 with a more efficient approach. Thus, this design gives the best performance over all. Due to asymmetry and a small rotation, Case 1 & 3 produce negative lifts at very small yaw angles when the system is active. Case 1 has the lowest lift coefficient when compared to other designs.

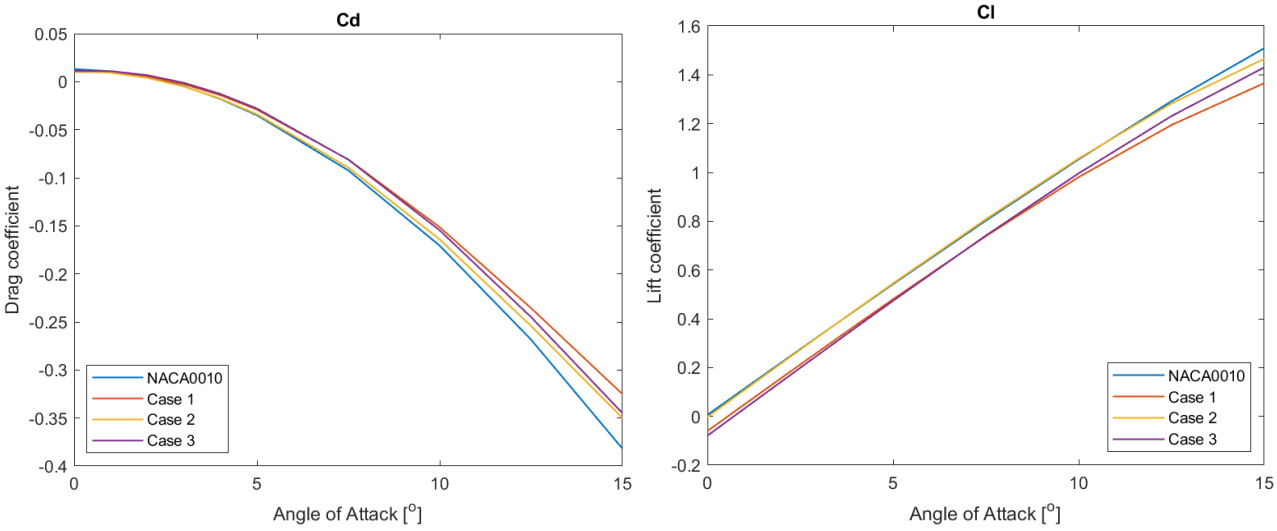

(a) *Coefficient of drag* (b) *Coefficient of lift*

Figure 3.31: *Comparison of the force coefficients for the generated active designs*

4 Wing and Pylon Study

The Purpose of the wing and pylon study is to analyse the effect of different pylon positions and profiles along with passive and active systems on the air flow around the wing. Three dimensional flow simulations are performed in STAR-CCM+ to find the optimum combination for maximum wing performance between 0° and +15° yaw angle. It is to be noted that as the wing and pylons are symmetric about XZ plane, the yaw angle scope reduces to 0° and +15°. This chapter highlights the numerical set up in STAR-CCM+ and the reasons for performing specific tests in the quest to find an optimum combination.

4.1 Simulation Overview

4.1.1 Coordinate System & Force Coefficients

The coordinate system used for the simulations can be seen from the wing and pylon isometric view in Figure 4.1. The pylons shown here are 24cm length NACA0010 pylons resting under the Aventador SV[1] wing. A modified airfoil is used for confidentiality purposes. Positive X direction is rearward, such that it would be downstream for a 0° flow. The pylon lying in the positive Y-direction is referred to as the right pylon throughout the report, while the pylon lying in negative Y-direction is the left pylon. For any angle between 0° and +15°, the left pylon would lie upstream and the right pylon lies downstream. The wing rests over the pylons in positive Z-direction.

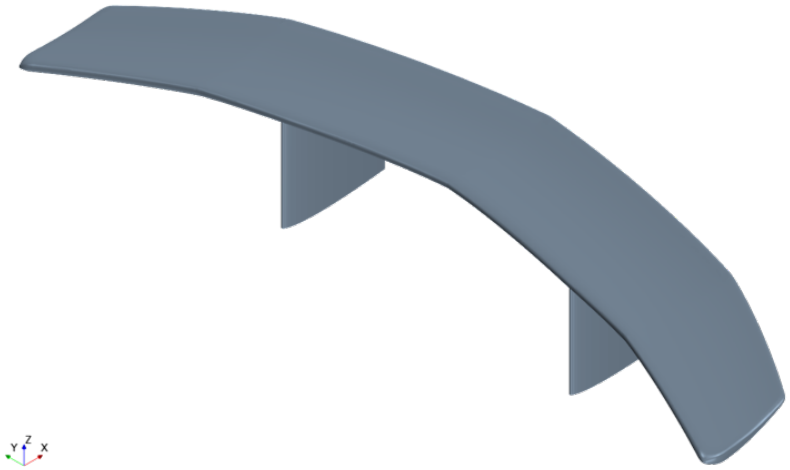

Figure 4.1: *Wing + Pylon Isometric view*

In Chapter 2, Airfoil Study, the force in Y-direction (F_y) was related to lift coefficient (C_L). In three dimensional flow, the force coefficient in Y-direction changes to the side force coefficient (C_S), and an additional Z-direction force (F_z) is introduced that relates to the lift coefficient. With the top view area of the wing as the reference area 'A', the equations for these two coefficients are as follows;

$$C_S = \frac{2 * F_y}{\rho * v^2 * A} \qquad (4.1) \qquad\qquad C_L = \frac{2 * F_z}{\rho * v^2 * A} \qquad (4.2)$$

4.1.2 Computational Domain

Defining an optimum computational domain around the object is important for a successful simulation. It must be large enough not to influence the object in focus, but not exceptionally large that it demands very high number of cells. As the simulation study scope does not exceed 15° yaw angle, we defined the domain to be 14m in length, 8m in both width and height. The wing assembly was placed such that it centered the domain along Y and Z axis, but left 10m length behind it in the X axis. Centring of the wing in Z-direction was a stakeholder requirement to ensure ground effect does not come into play. The front and right walls in Figure 4.2 indicate the flow inlet boundaries, and the left and rear walls are pressure outlets. The top and

bottom walls that complete the domain were set as symmetry planes. As the assembly is symmetric, the left and right walls did not swap boundary conditions to simulate $-15°$ yaw angle.

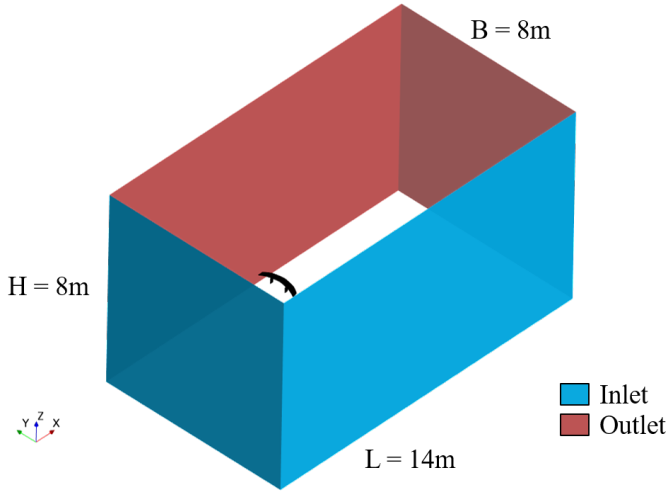

Figure 4.2: *Computational Domain & Boundaries*

4.1.3 Simulation Parameters

The boundary conditions and physics models need to be carefully defined and selected for the wing and pylon study. The inlet and outlet walls are highlighted in Figure 4.2. For the inlet wall, the conditions are the same as described for the 2D study in Section 2.1. The physics models selected are as follows:

- **RANS solver:** Reynolds-Averaged Navier Stokes solver was used for this simulation as computational requirements for detached/large eddy simulations are extremely high.
- **SST k-ω turbulence model:** A robust low Reynolds number turbulence model. Its capability to switch from k-ω to k-ϵ when needed makes it a popular turbulence model[13][17].
- **All y^+ Wall Treatment:** Selected for its robustness. Using 13 prism layers within $2mm$ thickness, the goal was to keep the y^+ values below 1.
- **Incompressible flow:** As the fluid velocity does not exceed Mach 0.3, constant density is assumed.
- **Steady flow:** This simulation is independent of time.
- **Coupled flow:** Benefits from Grid Sequence Initialising which helps to converge the solution faster.

4.1.4 Mesh Study

In a project where the number of potential simulations carried out were bounded by the project duration and allotted computational resources, it was important to expend lesser time meshing. Trimmer (Hexahedral) Mesher produces reliable results while taking lesser time than Polyhedral Mesher in generating volume mesh. Trimmer Mesh is renowned for its external aerodynamics application in the automotive industry[18][19]. Also, the Trimmer Wake Refinement option produces shape defined wake regions that ensured a robust mesh for varying yaw angles. The cell size used for the wake region is the base size mentioned further, while the wing target surface size was set as half the base size. The key to accurately control a trimmer mesh for the refinement zones is to ensure that the cell sizes are proportional to the base size by multiples of two. Refinement zones around the wing were implemented to ensure accurate capture of gradients. These volumetric refinements are evident in Figure 4.3. As the wing is placed far from any domain boundary, the wing surface refinement did not affect the domain surfaces. The prism layers were carried over from the 2D study, which captured the viscous boundary layers.

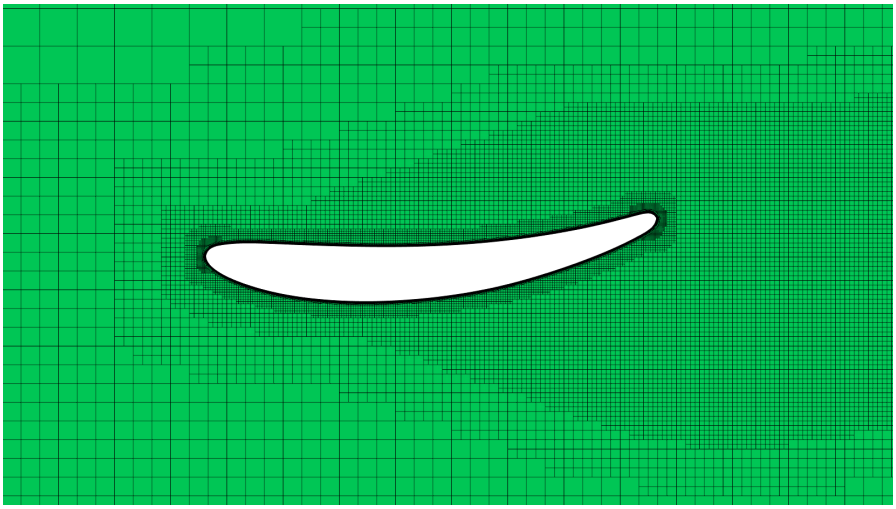

(a) *Mesh closer to the wing*

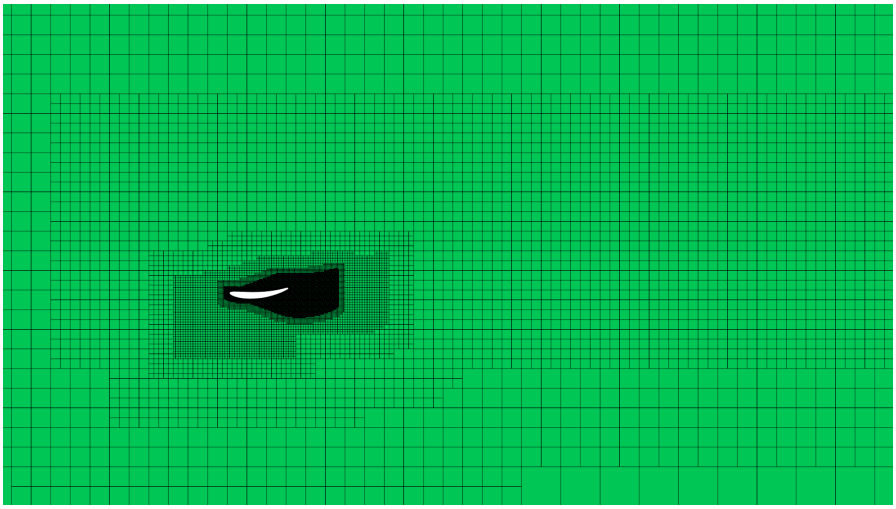

(b) *Far field meshes*

Figure 4.3: *Volume mesh around the wing at $Y = 0$, seen from left (-Y-direction)*

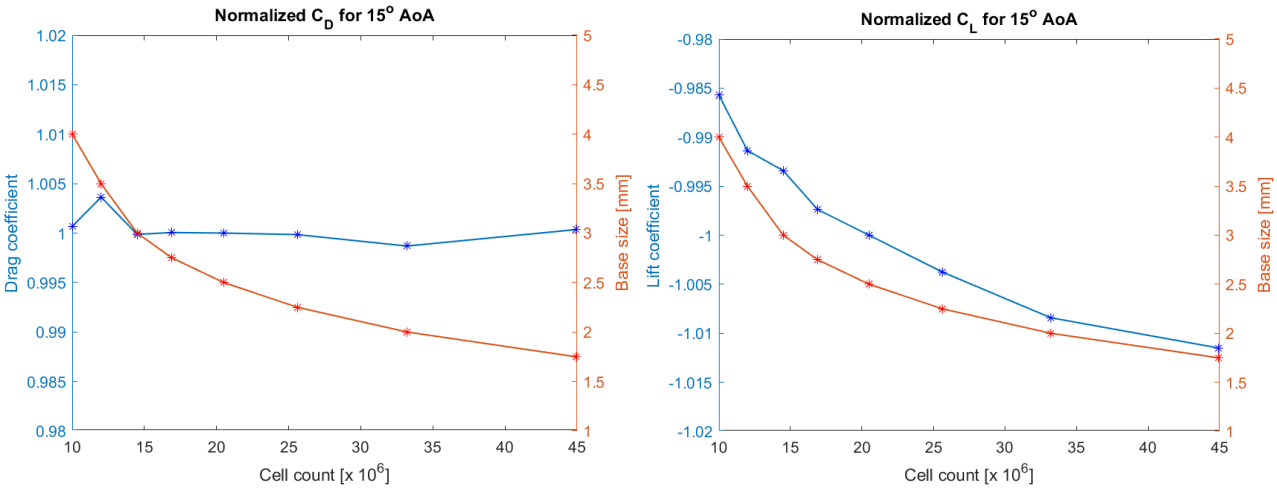

(a) *Drag force coefficient for 0° yaw*

(b) *Lift force coefficient for 0° yaw*

Figure 4.4: *Force coefficients vs number of mesh cells*

A mesh independence study was carried out on just the wing to ensure that the results do not vary significantly with progressive mesh refinement. Figure 4.4 shows normalized C_D and C_L values for $+15°$ yaw. The normalization here is done by the respective coefficient values for $2.5mm$ base size ($\approx$ 20.5 million cells). It was observed that at the maximum cell count tested ($\approx$ 45million cells), the change in C_L is less than 1%. The C_L values also start to flatten out as the number of cells increase. When the pylons are included in the mesh, the cell count increases drastically, thus, a 5 million cell count difference between $2.5mm$ and $2mm$ base size amplifies. Thus the $2.5mm$ base size mesh was judged to be appropriate for this study.

4.2 Pylon Length and Position Study

The purpose of this study is to arrive at an optimum combination of longitudinal translation and scaling down for the different pylons to provide attached flow around the wing. A reference wing and pylon assembly provided by Automobili Lamborghini S.p.A was used to determine the geometrical size and position of the new pylon profiles discussed in Chapter 3. Figure 4.5 shows an example positioning of the NACA0010 airfoil under the wing from the front view. With this reference positioning, the Y and Z axis translations were constrained, while, the position along X axis was varied for the position study. In a quest to obtain the optimum placement of the pylon, following three positions were tested;

- **Reference Position:** Starting the pylon from the reference point as shown in Figures 4.5 & 4.6. When the pylon was scaled down at this position, the trailing edge was pulled closer to maintain starting point.
- **Moved Rear:** Ending the pylon at the wing trailing edge. To scale down the pylon length, the leading edge was pushed back instead of pulling the trailing edge forward. An example of this positioning can be seen in Figure 4.7.
- **Moved Ahead:** Moving the pylons 5cm in front of the wing as seen in Figure 4.8. 5cm was chosen based off the chord lengths, a sensitivity analysis for positioning was not performed due to timeline constraints. This position required additional designing of the part over the wing. Like the reference position, the trailing edge was pulled closer when scaling down the pylon to maintain the starting point.

Figure 4.5: *Position of the left pylon (24cm length) along with reference point, from -X axis*

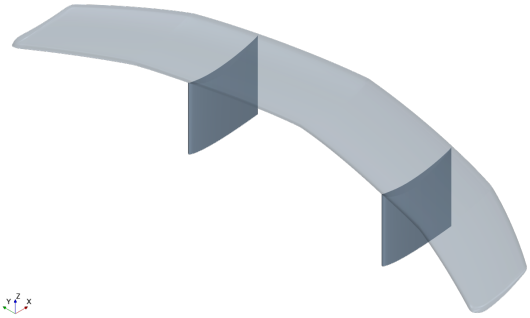

Figure 4.6: *24cm pylons at reference position*

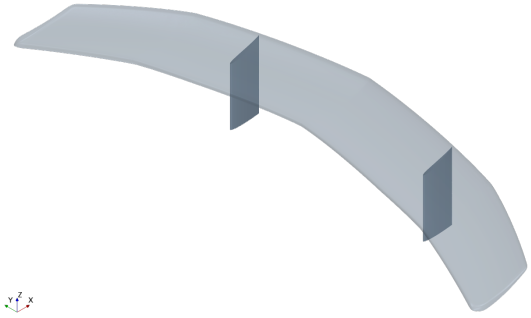

Figure 4.7: *10cm pylons moved rear*

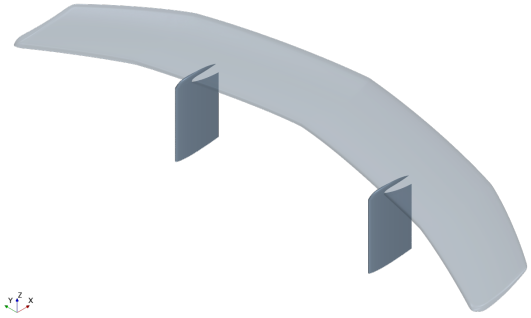

Figure 4.8: *15cm pylons moved ahead*

Limited by the chord length availability under the wing, the maximum pylon chord length was kept at $24cm$. With the height being taken from the reference pylon, it remained untouched. However, the length (X direction) and thickness (Y-direction) were proportionately scaled down to match the chord length requirements. Pylons with three varying chord lengths were tested;

- **24**cm chord length which is the maximum length available under the wing at the reference position. Example of this combination can be seen in Figures 4.1 & 4.6.
- **10**cm chord length to have minimum flow obstruction and lesser adverse pressure to overcome under the wing. This chord length was too small to include and passive and active systems and was set as the minimum length criteria.
- **15**cm chord length to essentially shorten the pylon length under the trailing edge of the wing while maintaining a length deemed long enough to accommodate passive and active systems even after scaling down the designs.

Table 4.1 lists out all the combinations of positioning and pylon chord lengths tested in STAR-CCM+ to achieve maximum wing performance. A total of 9 (3∗3) combinations were possible for each pylon design, however due to project timeline constraints, 6 configurations were tested since the remaining configurations were expected to underperform.

Pylon Location	**Chord Length**
Reference Position	24cm
	10cm
	15cm
Moved Rear	10cm
Moved Ahead	10cm
	15cm

Table 4.1: Pylon position & length combinations for simulation

5 Results & Discussion - Wing and Pylon Study

This chapter discusses the results for the 6 combinations mentioned in Table 4.1. In order to execute more simulations within the project timeline, the combinations were mainly analysed for NACA0010 and Case 2 pylon profiles at 0° and +15° yaw angles. For 0° yaw angle, discussing the C_D takes precedence while for +15° yaw, C_L and C_S hold more importance. However, all force coefficients are important and have not been neglected while deciding on the optimum combination. Once the combination showed promising results, the entire yaw sweep was performed for detailed comparison as discussed in Section 5.6.

It must be noted that the wing and pylon simulations performed during this study do not include a car body. As the pylons were designed considering that, there would be lower separation in a complete Lamborghini model when different flow physics are involved.

5.1 Reynolds Study

Before proceeding with the 3D simulations, a Reynolds study was performed on the 2D airfoils as different pylon sizes will be tested along with the wing. From Figure 5.1 it was observed that NACA0010 was severely affected by the changes in Reynolds number. Here, the lowest number signifies a $10cm$ pylon, while the middle number signifies a $15cm$ pylon at $140kmph$ flow. Case 2 pylon stalls when the size is reduced to 10cm, otherwise its performance is robust against a change in Reynolds number. However, it would be advisable to use a $15cm$ pylon for higher yaw angles, if not the $24cm$ pylon.

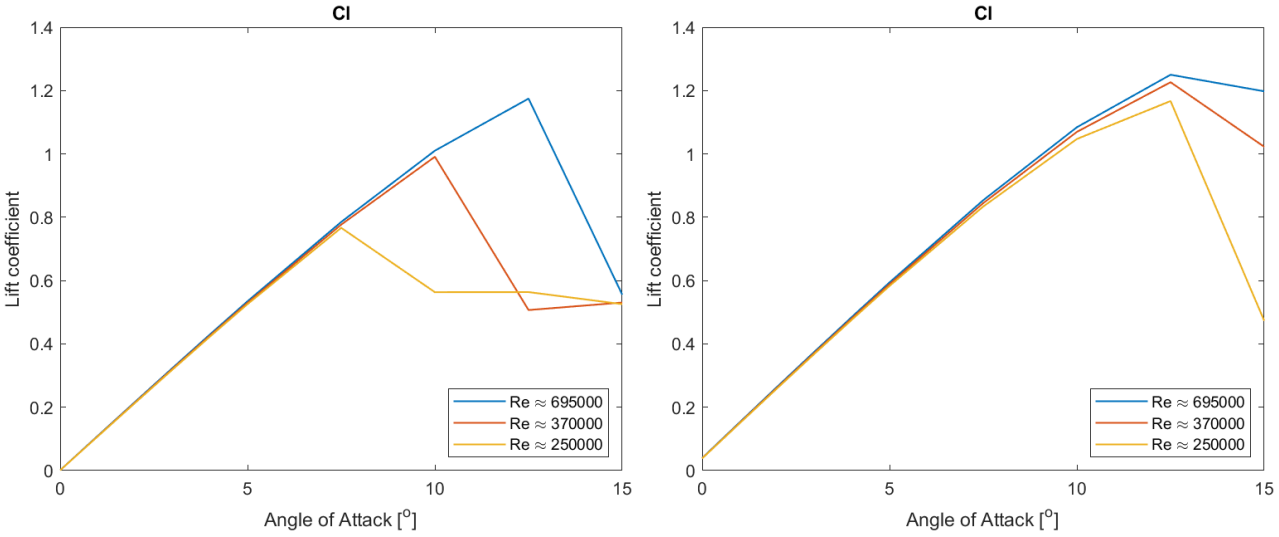

(a) *NACA0010* (b) *Case 2*

Figure 5.1: *Reynolds study of C_L for positive yaw angle sweep*

5.2 Wing Results & Normalization

To avoid disclosure of actual force coefficients, all the values mentioned henceforth have been normalized. The drag coefficient (C_D) was normalized by the C_D of just the wing at 15° yaw. The normalization of lift coefficient was done using the absolute C_L value of just the wing at 15° yaw. The absolute value was used to ensure same sign convention for forces, positive C_L denotes lift while negative C_L signifies downforce. This meant that the wing C_D and C_L results at 15° yaw would be 1 and -1 respectively as seen in Table 5.1. It was observed that both drag and downforce are greater at 0° air yaw than at +15° air yaw.

As just the wing produces negligible side force, C_S was normalized by the first 3D wing plus pylon simulation result presented (Table 5.2), the C_S of 24cm NACA0010 pylon at 15° air yaw. The annotation '(W+P)' is used to denote that the said value is for wing plus pylon, else it stands for just the wing alone. However

in this report, C_S was always considered for the wing and pylon combination, while C_L was considered only for the wing. Even though the variation in C_L is produced due to the pylon designs, the contribution of the pylon part itself to the lift force would be negligible. The drag coefficient is also considered for the '(W+P)' combination as the pylons have a significant contribution to the overall C_D. However, the pylons report slightly higher values due to abruptly ending pylons that cause small separations at the bottom.

Yaw Angle	$\mathbf{C}_D$	$\mathbf{C}_L$
0°	1.038	-1.069
15°	1	-1

Table 5.1: Results for the wing

5.3 Pylons at reference position

5.3.1 24cm pylon length

This combination was the first simulation performed to get an idea of the flow around the wing and pylons. Figures 5.2 & 5.3 show the region of total pressure equalled to zero around the wing and pylons. The $C_P = 0$ isosurface denotes the separation region that helps in visualizing the region of detached flow. These figures are oriented in such a way that the pylon on the left side of Figure is the left pylon, and the right pylon is on the right while the focus is on the underside of the wing. The direction of flow for +15° air yaw can be seen from Figure 5.3, where the flow separation is on the right side of the pylons, indicating that the flow is coming in from the left side.

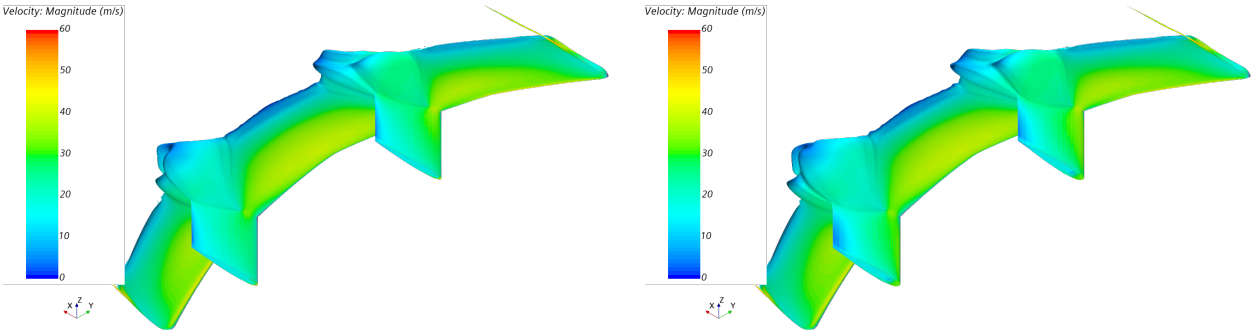

(a) *NACA0010* (b) *Case 2*

Figure 5.2: *Velocity magnitude over isosurface of* $C_P = 0$ *for 24cm pylons at 0° yaw*

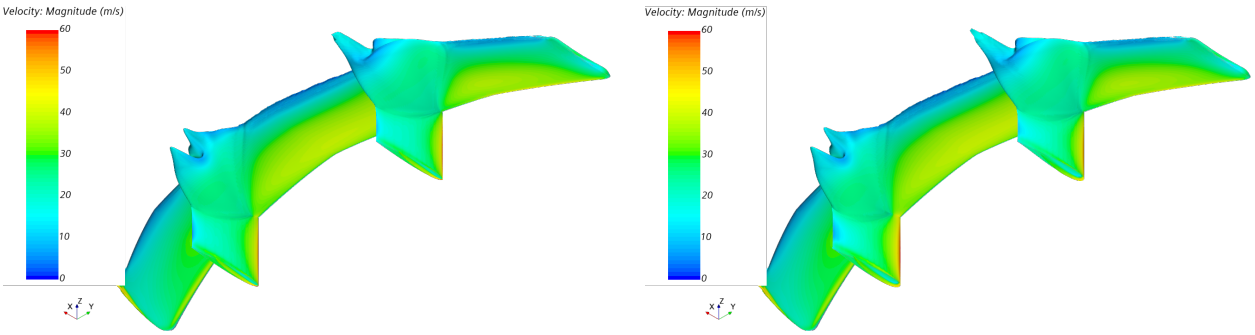

(a) *NACA0010* (b) *Case 2*

Figure 5.3: *Velocity magnitude over isosurface of* $C_P = 0$ *for 24cm pylons at +15° yaw*

For both 0° and +15° air yaw, we observe large separation regions. Due to this, the wing performance is worsened as the drag force increases while the downforce decreases. Thus, the approach using 24cm pylons was dropped for other positions. From the airfoil study, Case 2 was expected to perform better than NACA0010, however due to separation, the same trend was not reflected as seen in Table 5.2.

The passive and active systems designed during 2D study aimed to attach the flow on one side of the pylon. Due to symmetry of the wing assembly, flow around only one pylon would improve by implementing these systems. In this case, we observed flow separation on the right side of both the pylons. Thus, it was decided to move on to the next combination instead of controlling the flow as separation on one pylon was inevitable.

Yaw Angle	Pylon Design	C_D (W+P)	C_L	C_S (W+P)
0°	No Pylon	1.038	-1.069	-
	NACA0010	1.434	-0.835	-
	Case 2	1.521	-0.791	-
15°	No Pylon	1	-1	0.003
	NACA0010	1.321	-0.813	1
	Case 2	1.378	-0.809	0.959

Table 5.2: Results for 24cm pylon at reference position

5.3.2 10cm pylon length

Scaling down the pylon to 10*cm* length showed drastic improvement in the wing performance compared to 24*cm* length. A shorter pylon covers less area under the wing, especially towards the rear where the wing curls up and increases adverse pressure gradient. In this case, the pylon trailing section ends before increasing pressure demand for attached flow. Thus, the wing does not completely stall. For 0° airflow, slight detachments were observed towards the end of the wing, which resulted in lower $-C_L$ values. The importance of attached flow was seen when just one pylon with attached flow resulted in the 10cm pylons generating more side force than the 24cm pylons in the +15° yaw case. The NACA0010 right pylon showed slight detachment, resulting in lesser side force than Case 2. Thus, Case 2 was the better profile for this combination.

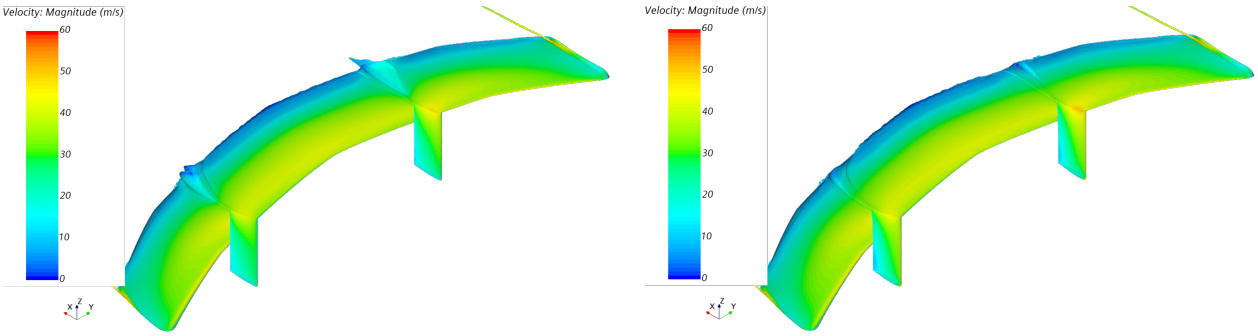

(a) *NACA0010* (b) *Case 2*

Figure 5.4: *Velocity magnitude over isosurface of* $C_P = 0$ *for* 10*cm pylons at* 0° *yaw*

Yaw Angle	Pylon Design	C_D (W+P)	C_L	C_S (W+P)
0°	No Pylon	1.038	-1.069	-
	NACA0010	1.102	-1.037	-
	Case 2	1.101	-1.048	-
15°	No Pylon	1	-1	0.003
	NACA0010	0.998	-0.894	1.164
	Case 2	0.971	-0.895	1.205

Table 5.3: Results for 10cm pylon at reference position

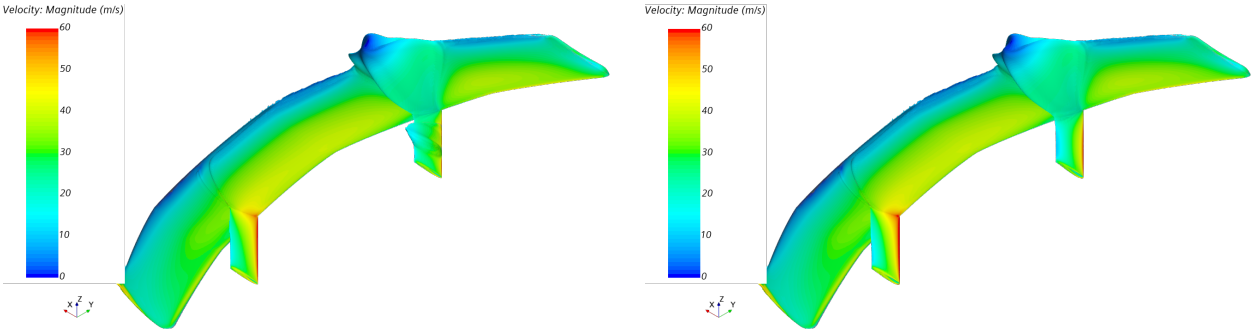

(a) *NACA0010* (b) *Case 2*

Figure 5.5: *Velocity magnitude over isosurface of* $C_P = 0$ *for* 10*cm pylons at* +15° *yaw*

5.3.3 15cm pylon length

From all the simulations discussed so far, it was confirmed that the right pylon was always creating a separated flow at +15° yaw angle due to the pylon positioning. Implementation of passive and active systems tried to mitigate the separation, but could not achieve ideal performance. For NACA0010 profile, the left pylon provides optimal performance with the attached flow. An active system with a $25m/s$ suction was added on the right side of the right pylon in an attempt to pull the flow. A slight improvement in forces was seen with the active system in place, however it was not enough and indicated towards changing the position. The interesting result here was that NACA0010 performed better than Case 2 at +15° yaw. From 2D study, NACA0010 should have detached flow at +15° while Case 2 is expected to produce a considerably attached flow. However, the larger thickness of Case 2 that resulted in outperforming NACA0010 in 2D study is the reason why it under-performed when attached to the wing. In this case, the flow stayed attached at the leading edge for both profiles, however, the flow needed to overcome greater adverse pressure gradient in Case 2 when it encountered the region under the wing. Thus, a sharper drop in thickness of Case 2 resulted in a detached flow for the left pylon.

The detached flow on the left pylon of Case 2 was addressed with active flow. Even though the assembly is symmetric about XZ plane, the active system gives freedom for asymmetry. In this case, Figure 5.6e, the active vent on the right side of the left pylon is blowing, while the mirrored vent on the left side of the right pylon is inactive. However, NACA0010 still performed better than Case 2 even with the assistance of additional systems. For the combination of passive and active system, the approach was to improve the flow around the pylon that was not aided by the passive system by creating a motorized suction. This improved the performance but not a significant improvement. The passive system aiding the left pylon was tested as well, but not documented as the right pylon with passive system performed better. In the end, this combination did not work out in terms of improving performance at +15° yaw angle, while the results in Table 5.4 showed that this combination resulted in an unacceptable performance at 0° yaw. The passive and active systems that aid the flow at higher yaw angles, perform worse at lower angles. Thus, those designs were not considered for 0° yaw angle.

Yaw Angle	**Pylon Design**	**C_D (W+P)**	**C_L**	**C_S (W+P)**
0°	No Pylon	1.038	-1.069	-
	NACA0010	1.346	-0.861	-
	Case 2	1.405	-0.835	-
15°	No Pylon	1	-1	0.003
	NACA0010	0.967	-0.906	1.384
	NACA0010, Active	0.915	-0.916	1.466
	Case 2	1.211	-0.835	0.973
	Case 2, Passive	1.169	-0.847	1.041
	Case 2, Active	0.997	-0.905	1.356
	Case 2, Pas+Act	1.130	-0.865	1.137

Table 5.4: Results for 15cm pylon at reference position

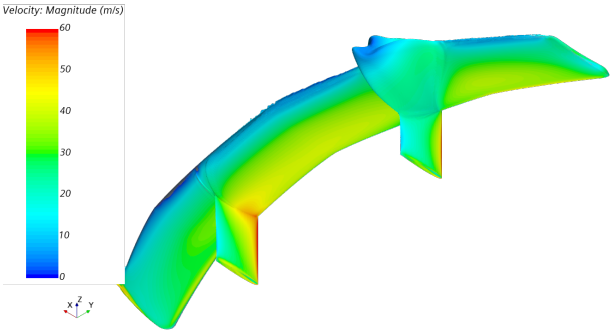

(a) *NACA0010*

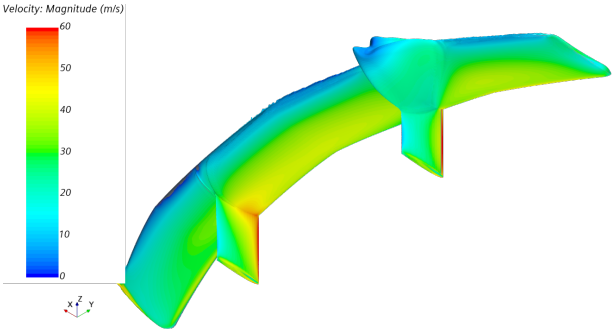

(b) *NACA0010, right with pylon active suction*

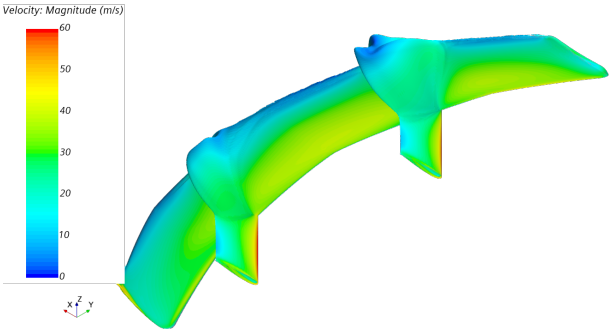

(c) *Case 2*

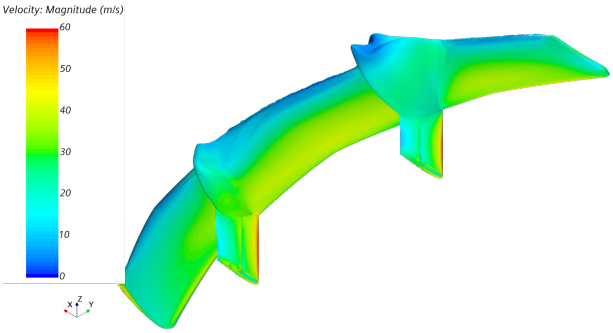

(d) *Case 2, passive aiding right pylon*

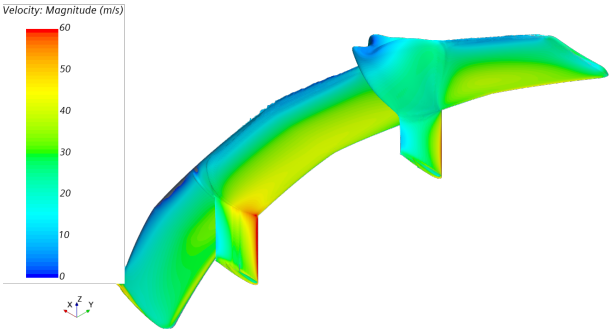

(e) *Case 2, active aiding left pylon*

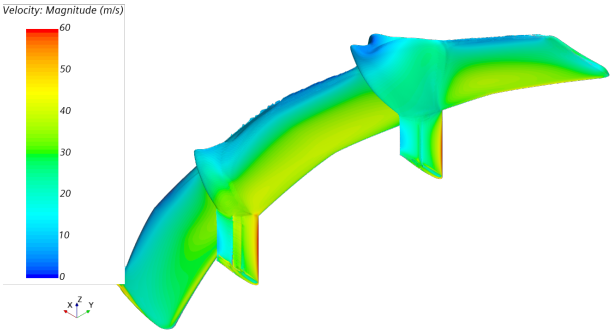

(f) *Case 2, passive aiding right + active suction on left pylon*

Figure 5.6: *Velocity magnitude over isosurface of* $C_P = 0$ *for* $15cm$ *pylons at* $+15°$ *yaw*

5.4 Pylons moved rearward

The pylon was moved to the rear end of the wing along the same X-axis with the idea that it would reduce the region of disturbed air under the wing. This approach was more inclined towards mitigating the reduction in performance caused by the pylons than improving the performance. The drag generated by the NACA0010 at $0°$ yaw was the lowest so far. While the downforce values for both the profiles had taken a hit when compared to $10cm$ pylons at reference position, presented in Table 5.3. The isosurfaces in Figure 5.7 show that, while the front part of the wing is undisturbed, the pylons and rear section of the wing had disrupted flow for $+15°$ yaw. When compared to the results of $10cm$ pylon at reference position, an improvement in downforce was observed. However, the drag and side forces worsen. The NACA0010 performs slightly better than Case 2 for this combination.

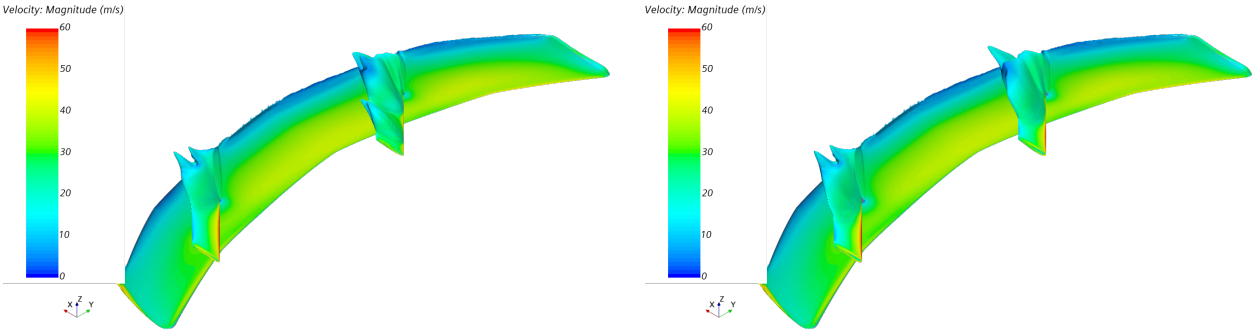

(a) *NACA0010* (b) *Case 2*

Figure 5.7: *Velocity magnitude over isosurface of* $C_P = 0$ *for* 10*cm pylons moved rear at* +15° *yaw*

Yaw Angle	Pylon Design	C_D (W+P)	C_L	C_S (W+P)
0°	No Pylon	1.038	-1.069	-
	NACA0010	1.091	-1.032	-
	Case 2	1.096	-1.038	-
15°	No Pylon	1	-1	0.003
	NACA0010	1.113	-0.934	0.671
	Case 2	1.132	-0.922	0.616

Table 5.5: Results for 10cm pylon moved rear, at +15° yaw

5.5 Pylons moved ahead

5.5.1 10cm pylon length - Lofted top

Moving the pylons 5*cm* in front of the wing showed drastic improvements in the force coefficients. This combination outperformed all the results discussed in previous sections. The performance at 0° yaw cannot be improved when a pylon is added unless a relative angle of attack exists between the pylon and flow. In the 2D study, it was observed that the drag coefficient increases for a few angles and then starts to reduce while the lift coefficient continues to rise. These are applicable if the flow is attached. So, for 0° yaw case, the results satisfy the study targets. For 15° yaw angle, both NACA0010 pylons showed a separation region. However, this was not seen on the wing, where the accelerated flow improved the downforce. Case 2, without separation on the right pylon, outperformed NACA0010 in all parameters.

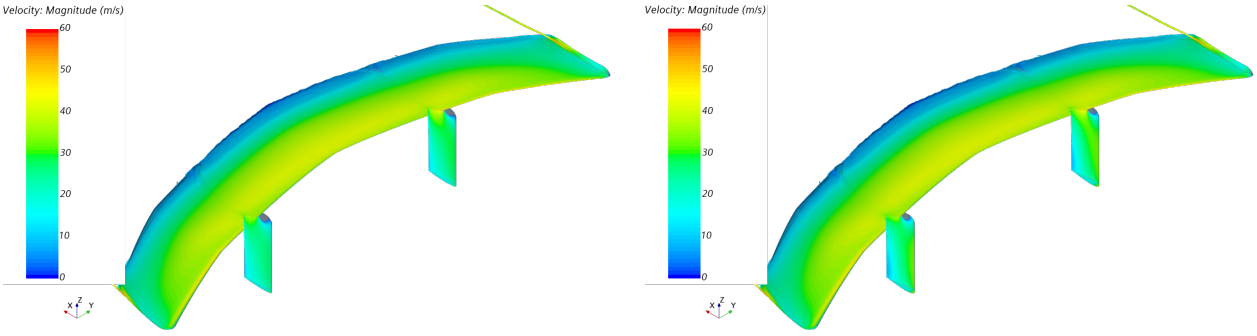

(a) *NACA0010* (b) *Case 2*

Figure 5.8: *Velocity magnitude over isosurface of* $C_P = 0$ *for* 10*cm pylons moved ahead at* 0° *yaw*

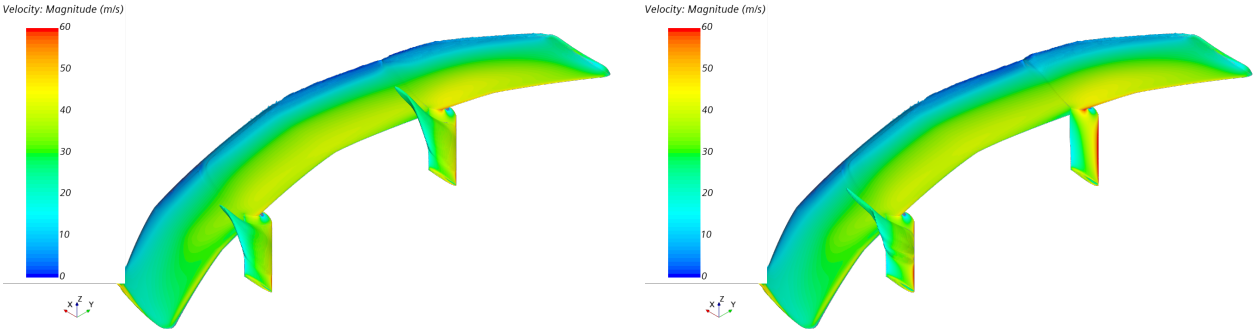

(a) *NACA0010* (b) *Case 2*

Figure 5.9: *Velocity magnitude over isosurface of* $C_P = 0$ *for* 10*cm pylons moved ahead at* +15° *yaw*

Yaw Angle	Pylon Design	C_D (W+P)	C_L	C_S (W+P)
0°	No Pylon	1.038	-1.069	-
	NACA0010	1.086	-1.067	-
	Case 2	1.091	-1.068	-
15°	No Pylon	1	-1	0.003
	NACA0010	0.889	-1.007	1.342
	Case 2	0.778	-1.010	1.452

Table 5.6: Results for 10cm pylon after moving ahead

5.5.2 15cm pylon length - Lofted top

Increasing the chord length to 15*cm* increased drag forces and lowered downforce for both profiles at 0° yaw when compared to 10*cm* length pylons. A pylon with longer chord length, is expected to perform better than a shorter pylon at +15°. For this combination, the NACA0010 created a small separation towards the right side trailing edge of the wing. Resulting in lower downforce than the 10*cm* pylon. Nevertheless, this design recorded the highest side force thus far. Case 2 recorded worse figures due to a significant separation as seen in Figure 5.11b. This was an unexpected result as Case 2 has greater robustness against yaw angles. A further discussion about this anomaly is presented in the following Section 5.5.3. Passive and active systems mitigated the separation for Case 2, but could not match up the results seen from the NACA0010 pylon.

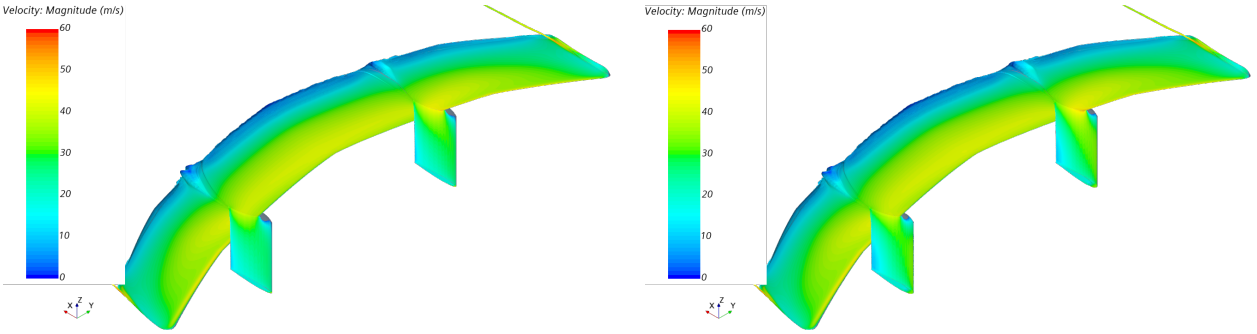

(a) *NACA0010* (b) *Case 2*

Figure 5.10: *Velocity magnitude over isosurface of* $C_P = 0$ *for* 15*cm pylons moved ahead at* 0° *yaw*

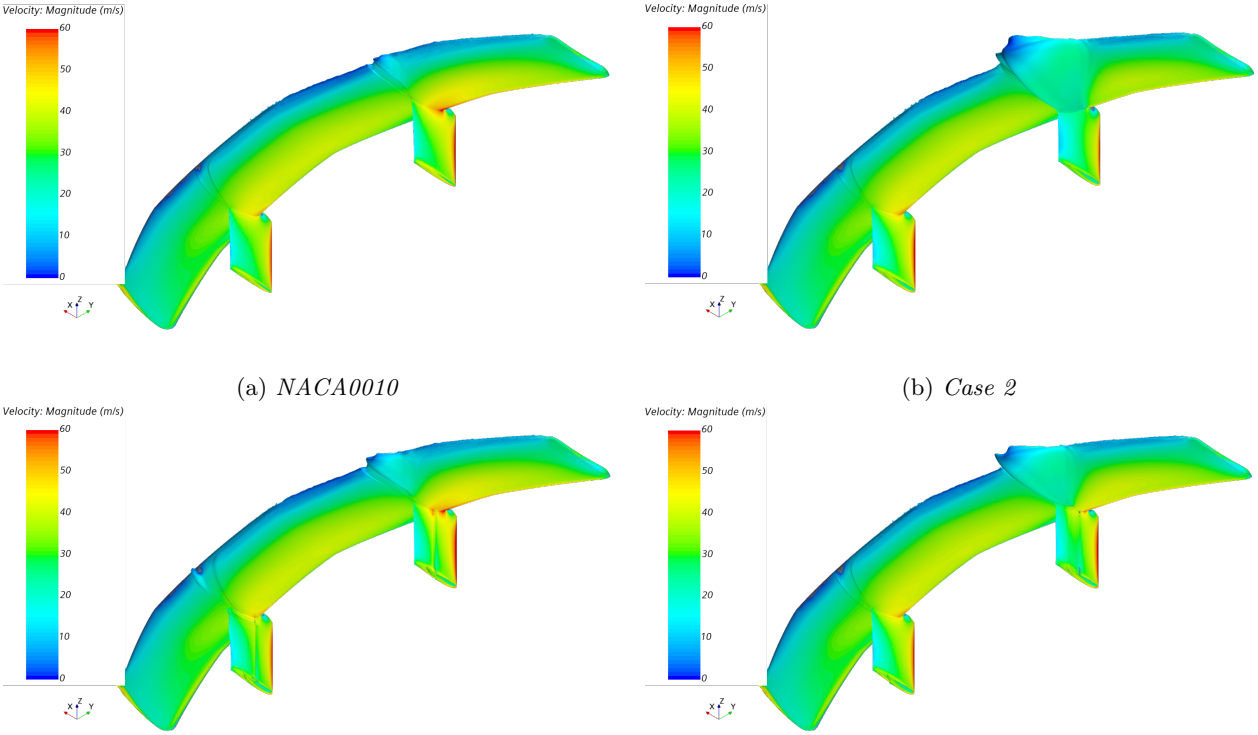

(a) *NACA0010*

(b) *Case 2*

(c) *Case 2, passive*

(d) *Case 2, active*

Figure 5.11: *Velocity magnitude over isosurface of* $C_P = 0$ *for* 15*cm pylons moved ahead at* $+15°$ *yaw*

Yaw Angle	Pylon Design	C_D	C_L	C_S (W+P)
0°	No Pylon	1.038	-1.069	-
	NACA0010, 15cm	1.116	-1.054	-
	Case 2, 15cm	1.121	-1.062	-
15°	No Pylon	1	-1	0.003
	NACA0010, 15cm	0.662	-1.002	1.945
	Case 2, 15cm	0.878	-0.912	1.671
	Case 2, passive, 15cm	0.713	-0.994	1.904
	Case 2, active, 15cm	0.766	-0.949	1.822

Table 5.7: Results for 15cm pylon after moving ahead

5.5.3 15cm pylon length - Sliced top

The top part of the pylon was designed arbitrarily to provide a smooth transition when the pylon was moved ahead. After seeing detached flow for Case 2 in Figure 5.11b, a deeper investigation was performed to find the cause. Figure 5.12b uses velocity streamlines to show flow separation for the Case 2 pylon at $+15°$ yaw angle. The curvature of the lofted top produced slightly accelerated flow and allowed considerable flow to move over the wing. A new top part of the pylon was designed that did not have a smooth curvature in the lateral (Y) direction. This sliced pylon was essentially a traverse cut on an extruded pylon. The lack of curvature over the pylon acted as an obstructive wall for the flow coming in from the right. Without a way to accelerate over the pylon, Figure 5.12b shows that the flow ended up accelerating around the leading edge of the pylon. The source of streamlines was kept constant for all images. With Q-criterion set at $800000/s^2$, the generation of vortices can be seen due to the sliced top in Figure 5.13a. When compared to the case of lofted top in Figure 5.12a, the clockwise vortex (positive value) is more prominent with a sliced top. This helped to maintain an attached flow and were visualized through streamlines. It was an interesting result that such a small part of the pylon affected the performance with such significance.

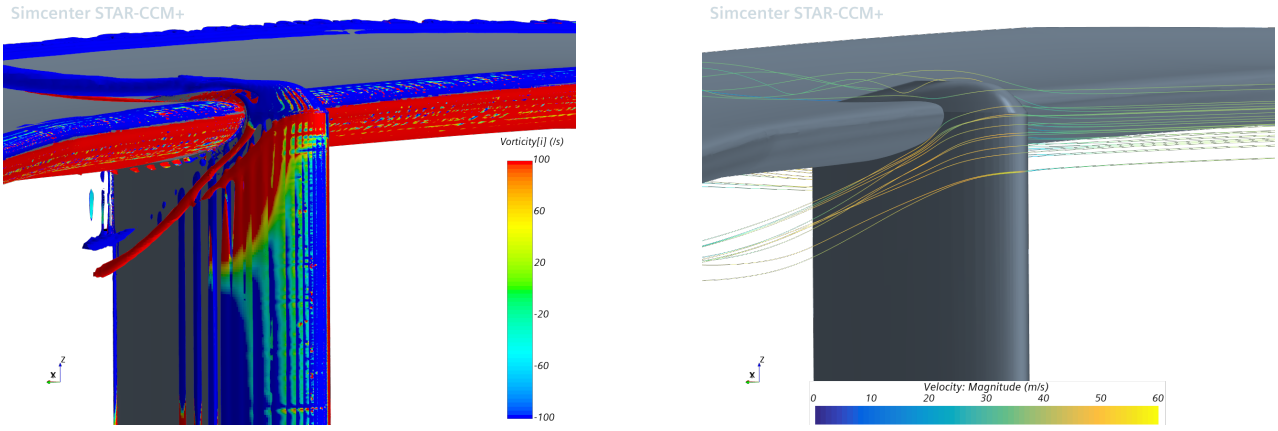

(a) *Vorticity* (b) *Streamlines*

Figure 5.12: *Case 2 right pylon with lofted top at +15° yaw*

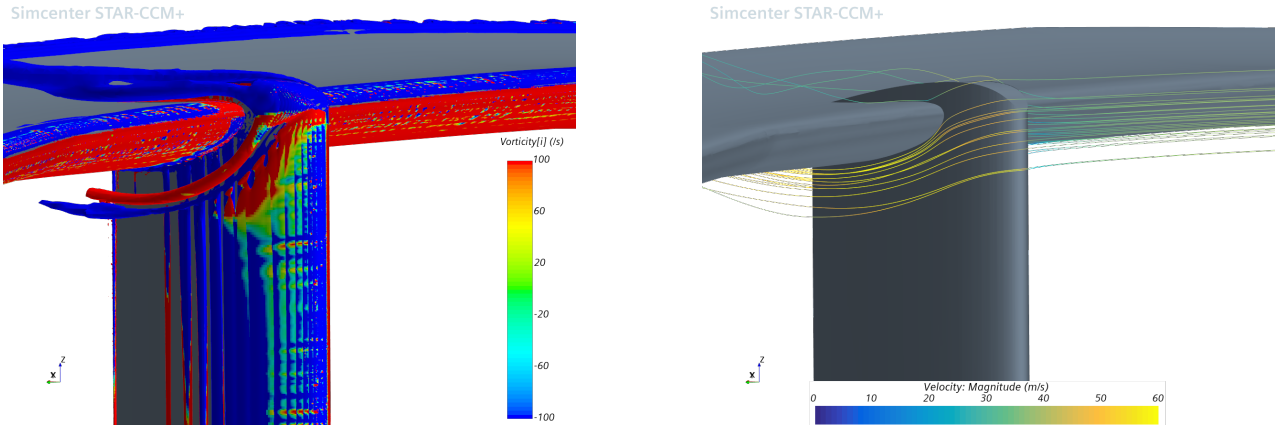

(a) *Vorticity* (b) *Streamlines*

Figure 5.13: *Case 2 right pylon with sliced top at +15° yaw*

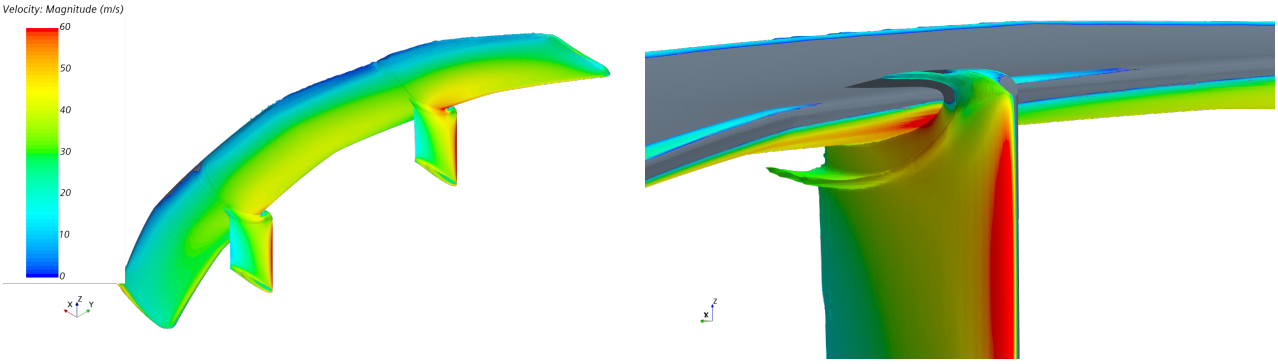

(a) *Case 2* (b) *Case 2, focus on right side of right pylon*

Figure 5.14: *Velocity magnitude over isosurface of $C_P = 0$ for 15cm pylon with sliced top at +15° yaw*

With the new top part designed, all four profiles discussed in 2D study were tested. Figure 5.14a shows the flow is attached around the Case 2 pylon. The two vortices generated due to sliced top (seen in Figure 5.13a) had opposite directions (clockwise and counter-clockwise) and the effect of the same can be noticed from the

disturbed $C_{P,total} = 0$ isosurface in Figure 5.14b. This phenomenon was common for all the profiles and was observed on the left pylons as well. The new sliced top helped in achieving maximum side force and down force at +15° yaw. The other three profiles performed very similarly as seen by the results in Table 5.8. When comparing the drag coefficients for NACA0010, the lofted top performed better. However, the sliced top improved downforce and side forces for NACA0010.

Yaw Angle	Pylon Design	C_D (W+P)	C_L	C_S (W+P)
0°	No Pylon	1.038	-1.069	-
	NACA0010	1.116	-1.053	-
	Case 2	1.132	-1.058	-
	Case 1	1.119	-1.059	-
	Case 3	1.132	-1.057	-
15°	NACA0010	0.674	-1.016	1.959
	Case 2	0.679	-1.019	2.000
	Case 1	0.672	-1.015	2.014
	Case 3	0.679	-1.017	2.014

Table 5.8: Results for 15cm pylons moved ahead with sliced top

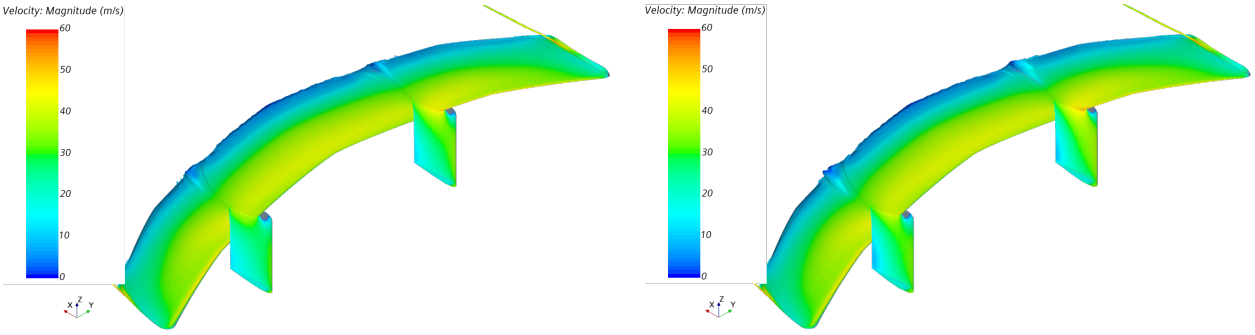

(a) *Case 1* (b) *Case 3*

Figure 5.15: *Velocity magnitude over isosurface of* $C_P = 0$ *for* 15cm *pylons with sliced top at* 0° *yaw*

Figure 5.15 shows isosurface for Case 1 and Case 3 at 0° yaw. The change in the top part of the pylon affected the results marginally as seen in Table 5.8, which also includes updated results for NACA0010 and Case 2 with sliced top. When compared to the lofted pylon results, the drag force had increased with the sliced top while the downforce reduced. Considering all the results produced by the sliced top, Case 2 seemed to perform better than others in most of the categories.

5.6 Comparison of best results

The combinations that produced the best results are tabulated in Table 5.9. When the position causes flow to detach, NACA0010 performs slightly better than Case 2. However, Case 2 outperformed NACA0010 in the combinations where the attached flow was observed.

Position	Length	Pylon Design	0° yaw		+15° yaw		
			C_D (W+P)	C_L	C_D (W+P)	C_L	C_S (W+P)
-	-	No Pylon	1.038	-1.069	1.000	-1.000	0.003
RP	10cm	Case 2	1.101	-1.048	0.971	-0.895	1.205
MA	10cm	Case 2	1.091	-1.068	0.778	-1.010	1.452
	15cm	NACA0010, lofted	1.116	-1.054	0.662	-1.002	1.945
	15cm	Case 2, sliced	1.132	-1.058	0.679	-1.019	2.000

Table 5.9: Best results for wing and pylon study

Even though the best performer at reference position (RP) performed worse than the moved ahead (MA) combinations in all the force coefficients tabulated, it was still included for when the reference position must be adhered to. It has low drag at 0° yaw, while the stalled pylon at 15° yaw does not make it an optimum combination. Mainly as the down force generation on the inner wheels during cornering would reduce due to detachment. This can be seen in Figure 5.16, where the negative position denotes the half with left pylon, and positive position is the other half. Without pylons, the general trend is that the lift distribution is greater towards the right half, which would denote the inner wheels while cornering. With the introduction of a pylon at the reference position, the right half lift forces get disrupted and the total down force generation reduces. It was observed during the sweep study that this combination resulted in separated flow beyond 5° yaw angle. Thus, it was not considered for sweep comparison in Figure 5.17.

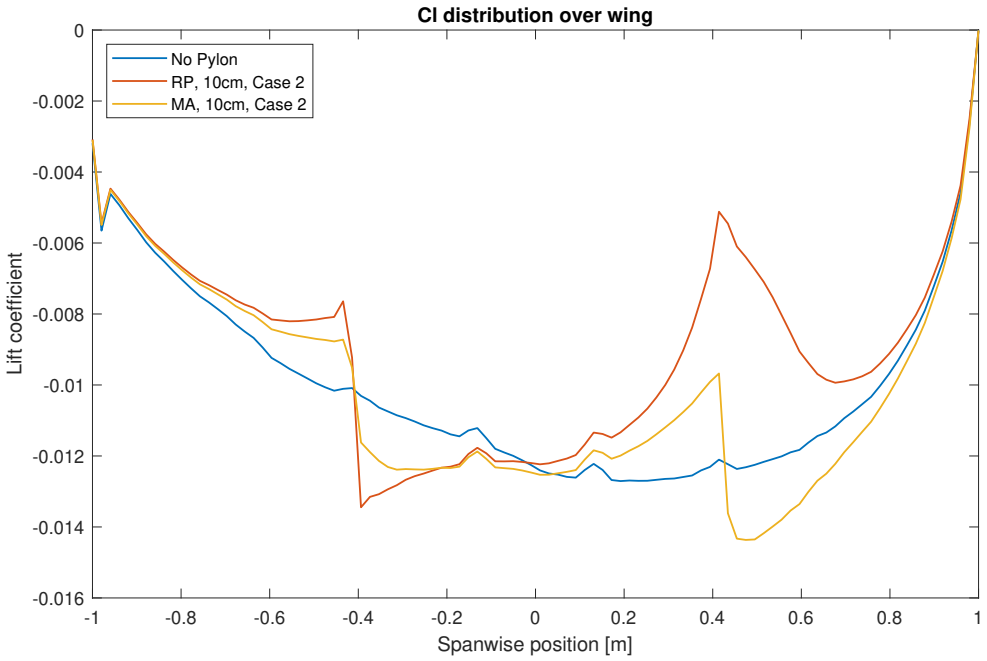

Figure 5.16: *Normalized spanwise lift distribution over the wing for +15° yaw angle*

The 10cm moved ahead pylon produced extremely good results at 0° yaw angle, however, this combination is questionable as it might not fulfill the safety requirements. For this reason, the design that provides moderate results for both angles, lofted NACA0010 was considered. Case 2 with the sliced pylon was the best performer for +15° yaw angle as it generated maximum downforce, with the second highest side force from all the simulations performed thus far. For 0° yaw angle, Case 2 sliced produces decent amounts of downforce at the cost of maximum drag amongst the best results.

As seen in Figure 5.17, a sweep comparison was performed on some combinations, to provide a deeper insight into the performance for various yaw angles. For lower yaw angles, inclusion of a pylon reduces performance in terms of C_D and C_L while the side force increases instantaneously above 0° yaw. The $10cm$ Case 2 pylon has the best performance in C_D between 0° and 10° yaw angles. This combination has the lowest side force generation for all yaw angles, while it has the best lift performance until the sliced Case 2 pylon takes top spot beyond 12.5° yaw. The sliced Case 2 and lofted NACA0010 perform similarly at lower angles, with the former being better at C_L and C_S. The drag and side forces do not see a drastic change when these two combinations are compared, however at 12.5° yaw, the trend for C_L of sliced Case 2 changes for the better as it starts to generate maximum downforce. This is where the effect of the sliced top part comes into play. The sliced Case 2 constantly generates the highest side force when compared to the best results.

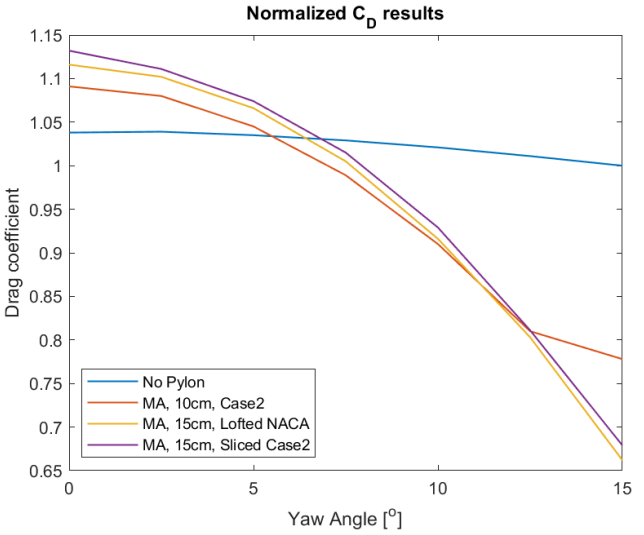

(a) C_D

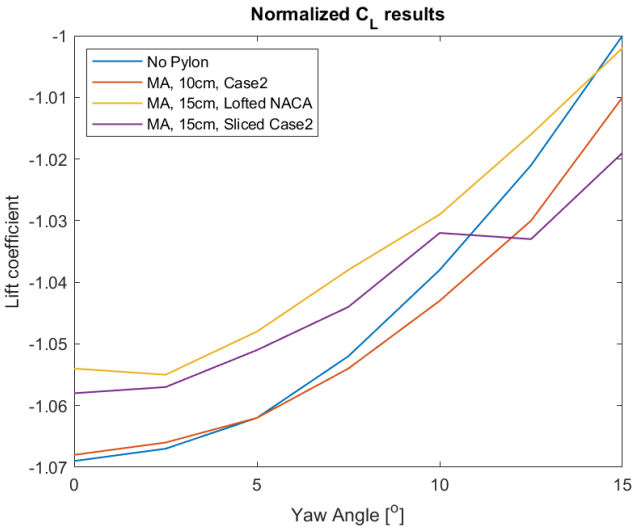

(b) C_L

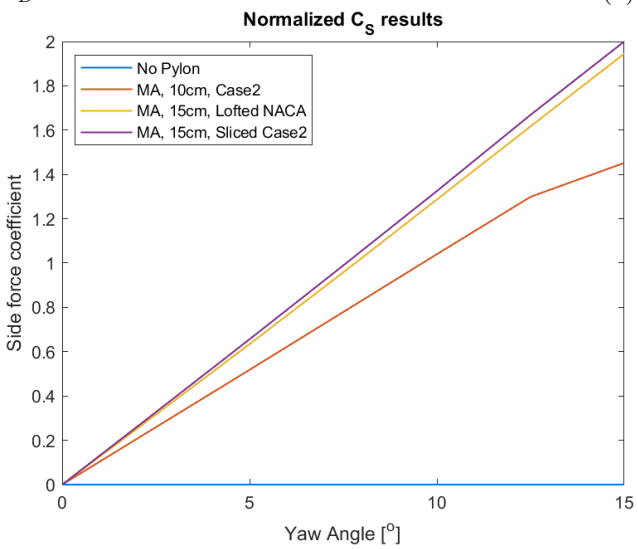

(c) C_S

Figure 5.17: *Force coefficients for a sweep study of best wing and pylon combinations*

5.7 Dependency on simulation conditions

The 3D simulations performed in this study had the wing and pylon assembly suspended mid-air along with a short pylon that ended abruptly. To test the effect of these two conditions, more simulations were performed at 15° yaw using the Case 2 pylon that was moved ahead with a sliced top (Figure 5.14). For the first simulation, the pylon length was increased substantially so that the bottom of the pylon would have no effect on the flow near the wing. As seen in Figure 5.18, this change caused slight reduction in performance at 15° yaw. The left pylon was observed to have lesser acceleration around the leading edge, thus causing the wing to drop performance. As the Reynolds study (Section5.1) suggested, the $15cm$ pylon tends to cause slight separation. However, as the right side (inner) has good performance, increasing the pylon length was acceptable in terms of downforce generation. The drop in performance can easily be rectified using active systems by aiding the flow around the upwind pylon.

The second simulation was performed by moving the wing and pylon assembly to the ground with slip condition. Thus, the wing rested at pylon's height distance from the ground. The pylon height here was set to be the same as the simulations performed in previous sections. Even though the right pylon resulted in detached flow, the total downforce was greater than the previous results. However, this increase in total downforce was due to the ground effect. Passive or active systems would be required to address the detachment.

The left side of the wing has highly accelerated air flowing under it, hence a greater downforce. The pylons were removed for another reference simulation in Figure 5.18. When comparing only wing results, a significant boost in performance was observed when the wing was moved closer to the ground.

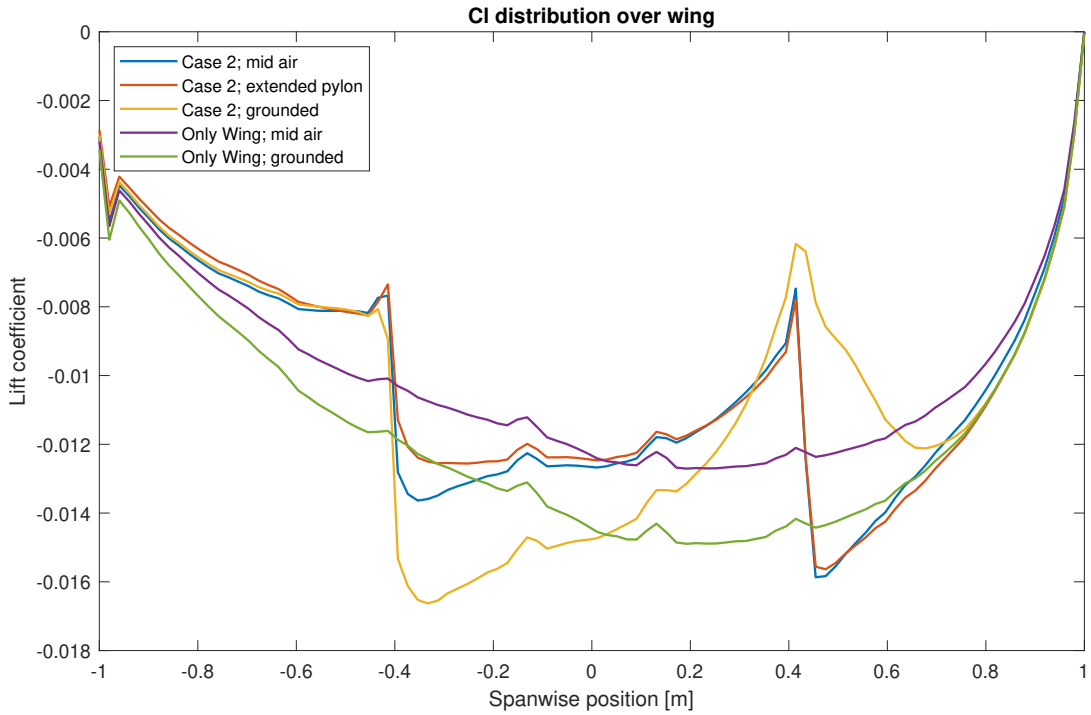

Figure 5.18: *Normalized spanwise lift distribution over the wing for* $+15°$ *yaw angle*

5.8 Importance of Passive & Active Systems

From the best results described in Section 5.6, it was observed that the closed pylons were capable of maintaining attached flow. And as we have noticed from the 2D study, if the flow stayed attached around a closed airfoil, those results got hampered when passive or active systems were implemented. However, providing attached flow around the pylons at high yaw angles is extremely difficult on a production car as the manufacturing and aesthetic constraints come into the picture. Section 5.7 showed the effects of boundary conditions on the flow attachment, which increased the need for implementation of passive and active systems.

From the Reynolds study in Section 5.1, it was seen that the profile's capability to provide attached flow reduced for a lower Reynolds number. Figure 5.19 shows a comparison of average lift forces for a sweep study at different Reynolds numbers, using 2D simulations. The two Reynolds numbers here, higher and lower, represent the airfoil study (Section 2) and $15cm$ pylon lengths respectively. When the Reynolds number was lowered, the effectiveness of these systems improved. The improvement in results due to passive or active systems for 15cm pylons at $+15°$ yaw angle was observed in Sections 5.3.3 and 5.5.2. Further analysis of Case 2 with a lofted top (Section 5.5.2) was carried out by performing a sweep study as seen in Figure 5.20. It was evident that these systems improve the performance at higher yaw angles, but perform worse at lower angles. Passive system showed improvement in 3D results when compared to the performance in the 2D study. However, the active system performed better than passive systems only at lower yaw angles and ended up performing worse beyond $5°$. The reason for reduction in active system performance came down to the design constraint of $3mm$ slot for active blowing. When the pylon was scaled down, the slot dimensions were unchanged, thus disturbing the optimized profile further. For a complete conceptual design, active system may perform better than the passive system.

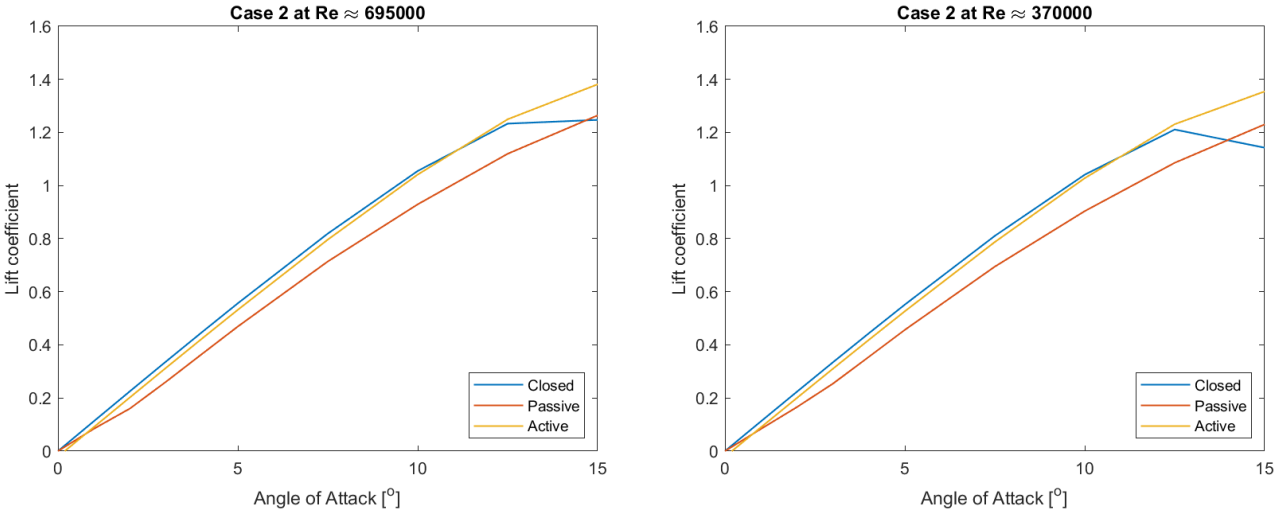

Figure 5.19: *Averaged C_L values for Case 2 at different Reynolds number*

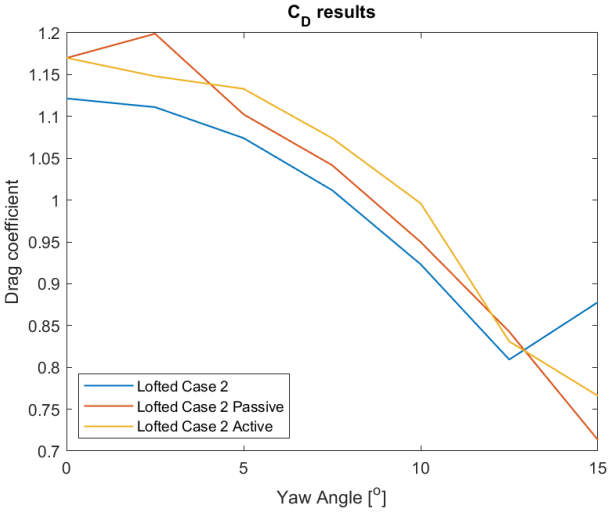

(a) C_D

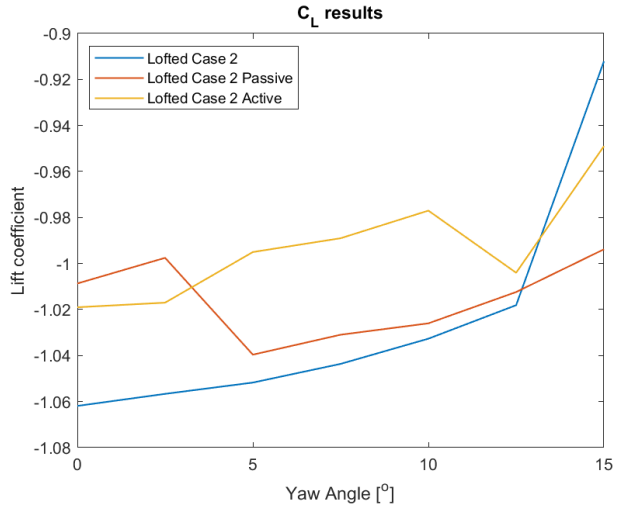

(b) C_L

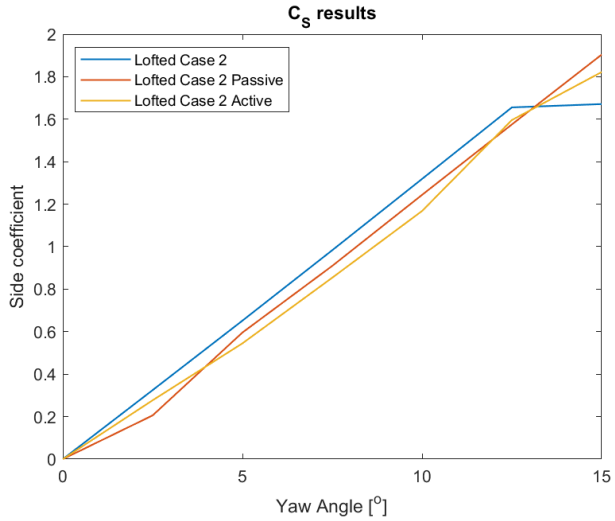

(c) C_S

Figure 5.20: *Force coefficients for a sweep study of moved ahead Case 2 pylon with lofted top*

6 Conclusion

The thin airfoils that produce lower drag forces at lower angles of attack showed signs of early separation when compared to thicker airfoils at higher yaw angles. The results from 2D study showed that asymmetric airfoils could be used to achieve greater averaged lift values. Out of the airfoils studied, Case 2 had the best performance overall. Case 1 was more efficient with the passive system, while Case 2 achieved optimum results with active blowing. Active system implementation on NACA0010 showed that motorized suction is more effective than the blowing (stagnation inlet) approach, but comes with the drawback of greater energy consumption. Passive systems have worse average lift forces when compared to active systems. However, passive systems do not require any additional energy in order to attach the flow at higher angles of attack. A trade-off is imminent and may be decided by the use case. With none of the closed airfoils producing completely attached flows at the specific Reynolds number, implementation of passive and active systems proved to be effective at higher yaw angles. The scope of using these systems may be increased when the Reynolds number is lower due to various reasons.

When the air flow in 3D simulations were attached, Case 2 pylon performed better than NACA0010. For placement of the pylon, best performances were observed when the pylons were placed in front of the wing. This helped the air to accelerate around the pylons before travelling under the wing at higher yaw angles. A $15cm$ pylon is optimum for this study scope as it provides good coverage against high yaw angles with less drag penalty in straights. If the yaw requirement is not large, choosing a smaller pylon size would be beneficial as it has the least negative impact in straights. If the pylons cannot be placed in front of the wing, moving the pylons rearward could be considered over the reference position due to sweep robustness.

The best results were achieved when the flow was completely attached around the closed pylons. However, due to styling constraints, it is very difficult to achieve attached flow for higher yaw angles as the pylon shapes are always a trade-off between aerodynamics and style department. Very often, the aerodynamics team must accept pylons with sharp edges for aesthetic reasons, making the optimized airfoils redundant. This is where the use of passive and active systems would be advantageous. Throughout the study it was shown that these systems improved the performance at higher yaw angles. While active systems did improve the performance when the flow was detached, passive systems have shown promising results by attaching the flow at high yaw angles without expending energy.

7 Future Work

The 3D simulations of wing and pylon combinations were performed with the assembly suspended mid-air. As seen in Section 5.7, the results vary when the boundary conditions differ. Testing out these combinations along with the car body could alter results slightly as it would produce different flow inclinations. Hence, this must be investigated. Wind tunnel tests could also be performed on down-scaled models to improve correlation with 3D simulations.

Deeper analysis may be performed on a few pylon parameters like;

- **Chord length.** Only three lengths were tested in this study, $10cm$, $15cm$ and $24cm$. Another length may provide better or more optimal sweep results.
- **Y axis positioning.** An investigation could also be carried out to analyse the effect of upstream pylon on the flow around the pylon placed downstream when positions are changed.
- **Moved ahead distance.** When the pylon was moved ahead by $5cm$, a sensitivity analysis might result in a position with better sweep performance. Especially when combined with varying chord length.
- **Moved ahead top part.** Various designs for the top part of the moved ahead pylons can be tested in combination with the position sensitivity analysis.

The slot for active flow in 3D simulations ran through the entire pylon height under the wing. This would disturb the pylon profile for the entire height, thus, under performing at lower yaw angles. By providing staggered and spaced out active flow control slots, this problem may be mitigated and might improve the flow attachment. This approach should be investigated and optimized in 3D simulations. Furthermore, passive and active systems could be implemented in an alternating manner, individually or combined, such that they can improve flows on both sides of the pylon. The boost in performance with this approach, if any, must outweigh the complexity in manufacturing such a system.

References

[1] *Lamborghini Aventador SuperVeloce*. URL: https://www.lamborghini.com/en-en/brand/masterpieces/aventador-superveloce (visited on 06/10/2021).

[2] Automobili Lamborghini S.p.A Ugo Riccio A. Torluccio. "Lamborghini Aventador SVJ Aerodynamics: Route to breaking the super sport car's record". *19th Stuttgart International Symposium*, pp. 469–470.

[3] Lamborghini. *Huracán Performante: How the ALA (Lamborghini Active Aerodynamics) works*. URL: https://www.youtube.com/watch?v=Ur4NLTqqWEw&ab_channel=Lamborghini (visited on 06/10/2021).

[4] Lamborghini. *Behind the secrets of the Aventador SVJ: ALA 2.0 Aerodynamic System*. URL: https://www.youtube.com/watch?v=dFQ5U0YzzDo&ab_channel=Lamborghini (visited on 06/10/2021).

[5] Oskar Pettersson Oskar Hellsten. A novel approach to the design of rear airfoil pylons on high performance car (2020). URL: https://hdl.handle.net/20.500.12380/301059.

[6] Justin Winslow et al. Basic Understanding of Airfoil Characteristics at Low Reynolds Numbers (104–105). *Journal of Aircraft* **55**.3 (2018), 1050–1061. DOI: 10.2514/1.C034415. eprint: https://doi.org/10.2514/1.C034415. URL: https://doi.org/10.2514/1.C034415.

[7] I.H. Abbott and A.E. Von Doenhoff. *Theory of Wing Sections, Including a Summary of Airfoil Data*. Dover Books on Aeronautical Engineering Series. Dover Publications, 1959. ISBN: 9780486605869. URL: https://books.google.se/books?id=DPZYUGNyuboC.

[8] Viorel Bostan, Marin Gutu, and Odainai Valeriu. Aerodynamic efficiency enhancement for asymmetric profiles. *MATEC Web of Conferences* **178** (July 2018). DOI: 10.1051/matecconf/201817806022.

[9] Simon McBeath. *Competition Car Aerodynamics, 3rd Edition*. 2017.

[10] AirfoilTools. *Airfoil plotter*. 2021. URL: http://airfoiltools.com/plotter/index (visited on 06/10/2021).

[11] Siemens. *Simcenter STAR-CCM+ 2020.3*. URL: https://www.plm.automation.siemens.com/global/en/products/simcenter/STAR-CCM.html (visited on 06/10/2021).

[12] MathWorks. *MATLAB*. URL: https://www.mathworks.com/products/matlab.html (visited on 06/10/2021).

[13] F. Menter. "Zonal Two Equation k-w Turbulence Models For Aerodynamic Flows". *23rd Fluid Dynamics, Plasmadynamics, and Lasers Conference*. DOI: 10.2514/6.1993-2906. eprint: https://arc.aiaa.org/doi/pdf/10.2514/6.1993-2906. URL: https://arc.aiaa.org/doi/abs/10.2514/6.1993-2906.

[14] Magnus Urquhart, Emil Ljungskog, and Simone Sebben. Surrogate-based optimisation using adaptively scaled radial basis functions. *Applied Soft Computing* **88** (2020), 106050. ISSN: 1568-4946. DOI: https://doi.org/10.1016/j.asoc.2019.106050. URL: https://www.sciencedirect.com/science/article/pii/S1568494619308324.

[15] Jeff Bezanson et al. Julia: A Fresh Approach to Numerical Computing (2017). URL: http://hdl.handle.net/1721.1/110125.

[16] Xiaoqiang Lu et al. An improved geometric parameter airfoil parameterization method. *Aerospace Science and Technology* **78** (2018), 241–247. ISSN: 1270-9638. DOI: https://doi.org/10.1016/j.ast.2018.04.025. URL: https://www.sciencedirect.com/science/article/pii/S1270963817304686.

[17] F. R. Menter. Two-equation eddy-viscosity turbulence models for engineering applications. *AIAA Journal* **32**.8 (1994), 1598–1605. DOI: 10.2514/3.12149. eprint: https://doi.org/10.2514/3.12149. URL: https://doi.org/10.2514/3.12149.

[18] *Mesh models in STAR-CCM+*. The Answer is 27. Nov. 21, 2013. URL: https://theansweris27.com/mesh-models-in-star-ccm/ (visited on 06/10/2021).

[19] Kynan Maley. "Best Practices: Volume Meshing". *South East Asian Conference*. 2012. URL: http://mdx2.plm.automation.siemens.com/sites/default/files/Presentation/SEA%20Conference%202012_CDadapco_VolumeMeshing_Used_KM.pdf (visited on 06/10/2021).

[20] Shivananda Sarkar and Shaheen Mughal. CFD Analysis of Effect of Flow over NACA 2412 Airfoil through the Shear Stress Transport Turbulence Model (July 2017).

[21] Syed Aftab et al. Turbulence Model Selection for Low Reynolds Number Flows. *PloS one* **11** (Apr. 2016), e0153755. DOI: 10.1371/journal.pone.0153755.

DEPARTMENT OF MECHANICS AND
MARITIME SCIENCES
CHALMERS UNIVERSITY OF TECHNOLOGY
Gothenburg, Sweden 2021
www.chalmers.se

CHALMERS
UNIVERSITY OF TECHNOLOGY